



Research paper

Discovery of 2-oxy-2-phenylacetic acid substituted naphthalene sulfonamide derivatives as potent KEAP1-NRF2 protein-protein interaction inhibitors for inflammatory conditions

Meng-Chen Lu^{a, b}, Hong-Li Shao^a, Tian Liu^a, Qi-Dong You^{a, b, *}, Zheng-Yu Jiang^{a, b, **}^a State Key Laboratory of Natural Medicines and Jiang Su Key Laboratory of Drug Design and Optimization, China Pharmaceutical University, Nanjing, 210009, China^b Department of Medicinal Chemistry, School of Pharmacy, China Pharmaceutical University, Nanjing, 210009, China

ARTICLE INFO

Article history:

Received 17 April 2020

Received in revised form

26 July 2020

Accepted 4 August 2020

Available online 22 August 2020

Keywords:

KEAP1-NRF2 pathway

Protein-protein interaction inhibitors

Oxidative stress

Inflammation

ABSTRACT

Nuclear factor erythroid 2-related factor 2 (NRF2) is a pleiotropic transcription factor which regulates the constitutive and inducible transcription of a wide array of genes and confers protection against a variety of pathologies. Directly disrupting Kelch-like ECH-associated protein 1 (KEAP1)-NRF2 protein-protein interaction (PPI) has been explored as a promising strategy to activate NRF2. We reported here the first identification of a series of 2-oxy-2-phenylacetic acid substituted naphthalene sulfonamide derivatives as potent KEAP1-NRF2 inhibitors. Our efforts led to the potent small molecule KEAP1-NRF2 inhibitor, **20c**, which exhibited a K_d of 24 nM to KEAP1 and an IC_{50} of 75 nM in disrupting KEAP1-NRF2 interaction. Subsequent biological studies provided consistent evidence across mouse macrophage cell-based and *in vivo* models that **20c** induced NRF2 target gene expression and enhanced downstream antioxidant and anti-inflammatory activities. Our study not only demonstrated that small molecule KEAP1-NRF2 PPI inhibitors can be potential preventive and therapeutic agents for diseases and conditions involving oxidative stress and inflammation but also enriched the chemical diversity of the KEAP1-NRF2 inhibitors.

© 2020 Elsevier Masson SAS. All rights reserved.

1. Introduction

The human body is constantly exposed to various reactive insults, represented by the electrophilic and oxidative chemicals [1]. On one hand, redox reactions and reactive species, including reactive oxygen species (ROS) and reactive nitrogen species (RNS), are important for many physiological processes [2], on the other hand, the imbalance between the production and the removal of these reactive species could disturb the cellular redox homeostasis [3]. Excess oxidative chemicals can directly damage nucleic acids, lipids and proteins and induce the oxidative stress. Constant

oxidative stress has been closely associated with a number of chronic and inflammatory disease states, such as neurodegenerative diseases, chronic kidney disease, obstructive pulmonary disease, atherosclerosis and cancer [4–6]. There are multiple antioxidative and cytoprotective mechanisms in cells, and enhancing cellular defense system is a possible way to develop therapeutic agents of such diseases.

Nuclear factor (erythroid-derived 2)-like 2 (NRF2), a transcription factor protein with a basic leucine zipper DNA binding motif, is the predominant regulator of the cellular defending system. NRF2 induces transcription of various xenobiotic metabolizing enzymes and antioxidant proteins to maintain a stable internal environment [7]. Moreover, nuclear NRF2 can directly antagonize transcription of inflammatory factors [8,9]. The crucial role of NRF2 in anti-inflammation has also been intensively linked to its interplay with the redox-regulated transcription factor nuclear factor kappa B (NF- κ B) [10]. The NRF2 and NF- κ B pathways are proposed to counterbalance each other's activity via PPIs or through secondary messenger effects. The NRF2-ARE pathway antagonizes NF- κ B mediated transcription by inhibiting I κ B α degradation. Conversely,

* Corresponding author. State Key Laboratory of Natural Medicines and Jiang Su Key Laboratory of Drug Design and Optimization, China Pharmaceutical University, Nanjing, 210009, China.

** Corresponding author. State Key Laboratory of Natural Medicines and Jiang Su Key Laboratory of Drug Design and Optimization, China Pharmaceutical University, Nanjing, 210009, China.

E-mail addresses: youqd@163.com (Q.-D. You), jiangzhengyucpu@163.com (Z.-Y. Jiang).

Abbreviations

NRF2	Nuclear factor erythroid 2-related factor 2
KEAP1	Kelch-like ECH-associated protein 1
PPI	protein-protein interaction
ARE	antioxidant response element
ROS	reactive oxygen species
RNS	reactive nitrogen species
CUL3	Cullin3
LPS	lipopolysaccharide
FP	Fluorescence Polarization
ITC	Isothermal Titration Calorimetry
BLI	biolayer interferometry

qRT-PCR	quantitative real-time PCR
HO-1	Heme oxygenase 1
NQO-1	NAD(P)H dehydrogenase (quinone) 1
GCLM	glutamate-cysteine ligase regulatory subunit
SOD	superoxide dismutase
GSH-Px	glutathione peroxidase
MPO	myeloperoxidase
IL-1 β	interleukin-1 β
TNF- α	tumor necrosis factor α
NO	nitric oxide
DXM	dexamethasone
IFN- γ	interferon- γ .

NF- κ B can suppress transcription of NRF2-ARE dependent genes by preventing CREB binding protein (CBP) from binding to NRF2 and facilitating recruitment of histone deacetylase 3 (HDAC3) to MafK [11,12]. Besides, NRF2 activation also enhances antioxidant defense system, increases HO-1 expression and alters GSH homeostasis, which eliminate ROS and therefore inhibits ROS mediated NF- κ B activation [13,14]. Thus, NRF2 activation could be a viable way to antagonize stress and inflammation related disorders [15–18].

Cellular content of NRF2 is mainly controlled by the E3 ligase adaptor protein, Kelch-like ECH-associated protein 1 (KEAP1) in a redox sensitive manner. Under normal conditions, KEAP1 functions as a substrate adaptor for a Cul3-based E3 ubiquitin ligase, constantly targeting Nrf2 for ubiquitin-dependent degradation. Upon oxidative and electrophilic stresses, KEAP1 functions as a sensor for the stress signals and loses its activity to interact with NRF2, resulting in reduced degradation of NRF2 [19–21]. Then, newly synthesized NRF2 protein can translocate to the nucleus and regulate the transcription. This manner of NRF2 activation inspires the development of electrophilic NRF2 activators, and some electrophiles have been proven to covalently modify sensitive cysteine residues of KEAP1 [22]. However, the targets of these electrophiles could be promiscuous, which makes it difficult to clarify the selectivity and the intact mechanism of action. Therefore, directly disrupting the KEAP1-NRF2 protein-protein interaction (PPI) have been proposed as a new avenue for NRF2 activation therapy [23–25].

In recent years, the development of KEAP1-NRF2 PPI inhibitors have made much progress [26–30]. Various screening approaches have been identified [31] and peptide inhibitors with diverse amino acid residues have been developed to elucidate the interface of the KEAP1-NRF2 PPI [32–38]. Moreover, small-molecular KEAP1-NRF2 PPI inhibitors have also been reported [39–46] and some molecules have achieved high potency [47–52]. The therapeutic potential of KEAP1-NRF2 inhibitors has also been explored in several *in vivo* disease models, including colitis [53], retinal ischemia-reperfusion injury [54], Alzheimer's disease [55] and inflammatory kidney disease [56].

Our group reported the first small molecule inhibitor, **1**, with nanomolar potency for KEAP1 binding and KEAP1-NRF2 inhibition [47]. Based on the crystallographic information of the reported naphthalene-1,4-sulfonamide based hit **2** [57], we introduced *N*-acetic acid groups to mimic the key Glu79 and Glu82 in the NRF2 ETGE domain, successfully obtaining compound **1** (IC₅₀ = 28.6 nM in a fluorescence polarization (FP) assay) [47] that fulfills all the five sub-pockets of KEAP1. Further drug-like property optimization of **1** gave analogs represented by **3** and **4** [58,59]. These efforts inspired the development of various 1,4-diaminonaphthalene-based KEAP1-NRF2 inhibitors reported in recent years [59–61].

ENREF_43In this study, we rationally designed a series of 2-oxy-2-phenylacetic acid substituted naphthalene sulfonamide derivatives as potent KEAP1-NRF2 inhibitors and identified that the 1,4-diaminonaphthalene substituted pattern is unnecessary for inhibiting KEAP1-NRF2 interaction. The represented compound **20c** exhibited a *K_d* of 24 nM to KEAP1 and an IC₅₀ of 75 nM in disrupting KEAP1-NRF2 interaction. **20c** induced the transcription activity of NRF2-antioxidant response element (ARE) in the ARE luciferase reporter assay and elevated both the mRNA and protein level of NRF2 and NRF2-regulated genes in macrophage cells. The activation of NRF2-regulated cyto-protective system by **20c** significantly antagonized the lipopolysaccharide (LPS) induced inflammatory conditions in cellular and *in vivo* models.

2. Results and discussion

2.1. Rational design and synthesis of 2-oxy-2-phenylacetic acid substituted naphthalene sulfonamide derivatives as KEAP1-NRF2 PPI inhibitors

In recent years, the KEAP1-NRF2 PPI inhibitors with a 1,4-diaminonaphthalene core have been extensively reported (Fig. 1A). The X-ray structure of the diacetamide-substituted compound **5** with KEAP1 fully confirmed the binding pattern of this scaffold (Fig. 1B and C) [60]. Compound **6** (IC₅₀ = 0.14 μ M), with only one sulfonamide group, was the first asymmetric compound of this scaffold [61]. Very recently, we reported the first identification of amino acids as preferred substituents to design potent KEAP1-NRF2 inhibitors, obtaining **7** with an IC₅₀ of 43 nM [62]. Taken together, these studies clearly revealed the five sub-pockets model of the KEAP1 cavity [63] and it is worthwhile to seek out novel agents suitable for the KEAP1-NRF2 interface.

Our previous studies have demonstrated the necessity of making multiple polar interactions with key Arg residues in the P1 and P2 polar sub-pockets of KEAP1. In this study, we retained the diacetic acid moiety but replaced one of the phenyl sulfonamide group with the hydroxyl group, resulting in compound **8**. The docking simulation showed that the oxyacetic acid group could occupy the P1 sub-pocket and form electrostatic interactions with Arg483 and Arg415. Then, **8** was synthesized and tested for KEAP1-NRF2 interaction inhibitory activity. Compound **8** showed moderate KEAP1-NRF2 inhibition activity (IC₅₀ = 8.19 μ M), which confirmed the suitability of the oxyacetic acid group in KEAP1-NRF2 inhibitor design. Of note, in the structure of compound **1**, the sulfonamide group can restrict the conformation of the acetic acid group; however, in the structure of **8**, the oxyacetic acid group is free to rotate and unable to occupy the P4 sub-pocket. In order to interact with the P4 sub-pocket, a hydrophobic benzene ring was

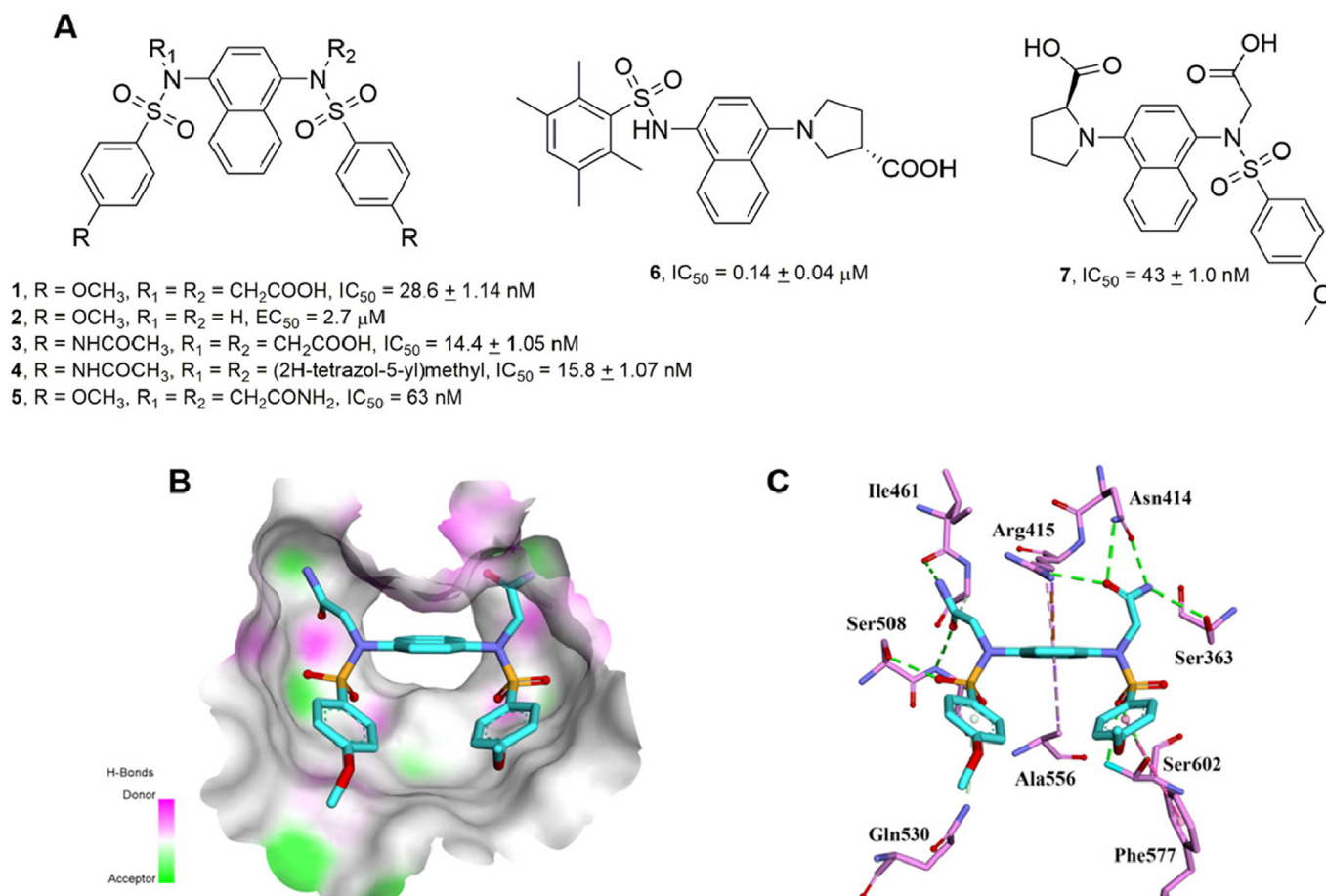


Fig. 1. Published 1,4-diaminonaphthalene-based KEAP1-NRF2 PPI inhibitors. (A) Chemical structures of known 1,4-diaminonaphthalene-based KEAP1-NRF2 PPI inhibitors. (B) Binding surface depiction of **5** with KEAP1 (PDB code: 4XMB). (C) Interaction mode of **5** with KEAP1 (PDB code: 4XMB). Hydrogen bonds are represented by green dashed lines, the electrostatic interactions are represented by orange dashed lines, and the hydrophobic interactions are represented by pink dashed lines. The carbon atoms of small molecules and KEAP1 residues are colored cyan and purple, respectively. (For interpretation of the references to color in this figure legend, the reader is referred to the Web version of this article.)

introduced to the methylene group in the oxyacetic acid group and resulted in **14a** with a significant increase in KEAP1-NRF2 inhibition activity (IC₅₀ = 2.28 μM). The docking study showed that **14a** could fulfill all the five sub-pockets of KEAP1: the oxyacetic acid group in the P1 sub-pocket retained the original strong polar interactions with Arg415 and Arg483 and the other carboxyl group in the P2 sub-pocket could make polar interactions with Arg415 and Arg380; the two hydrophobic benzene rings formed the π-π stacking interactions with Tyr525 and Tyr334 in the P4 and P5 sub-pockets; the naphthalene ring scaffold kept the cation-π interactions with Arg415 and Ala556 in the P3 sub-pocket to stabilize the binding conformation and the other part of the molecule can interact with KEAP1 in a similar way as the lead compound **1**. However, it cannot be ignored that this structure modification led to a significant decrease in activity compared to compound **1**, further comprehensive structure-activity relationship studies should be conducted to improve the activity.

2.2. Structure-activity relationships studies of **14a**

2.2.1. Substituent transformation on the side chain phenyl ring in the P5 sub-pocket

As shown in Fig. 2B, **14a** might not fully occupy the P5 sub-pocket, with only the hydrophobic benzene ring forming the π-π stacking interaction with Tyr334. Therefore, the substituents on the sulfonamide-substituted phenyl group of **14a** were chosen as the

optimization sites. We synthesized 14 compounds (**14b** ~**14o**) and systematically evaluated the effects of the different substituents on KEAP1-NRF2 PPI inhibition activity.

As shown in Table 1, the substituents on the sulfonamide-substituted phenyl ring had significant effects both on the KEAP1-NRF2 PPI inhibitory activity and the cellular NRF2-ARE induction activity. Generally, removal of the terminal methoxy group resulted in **14b** with a dramatic decrease in activity (IC₅₀ = 17.78 μM); the electron-donating substituents (**14a**, **14c** ~**14f**) exhibited better performance compared to electron-withdrawing (**14g** ~**14k**) and halogen substituents (**14l** ~**14n**).

In the exploration of the electron-donating substituents, we found that the *p*-methoxyl substituent (**14a**, IC₅₀ = 2.28 μM) was slightly more potent than *p*-methyl (**14c**, IC₅₀ = 2.69 μM). Introduction of the *meta*-methoxyl group gave **14e** (IC₅₀ = 2.30 μM), which is less potent than *para*-methoxyl, indicating that the hydrophobic groups were unfavorable in the meta-position. Noteworthy, the 2,4,6-trimethyl substituted compound **14f** exhibited the most excellent performance (IC₅₀ = 0.58 μM), likely because the *ortho*-methyl introduction enhanced the hydrophobic interactions in the P5 sub-pocket, which is supported by the docking simulation (Fig. 3A). An increase in potency by 2-naphthyl substitution (**14o**, IC₅₀ = 0.78 μM) also indicated that large hydrophobic group in this site is preferable for the KEAP1-NRF2 PPI activity.

On the whole, in the exploration of the substituents in the P5 sub-pocket, we obtained the most potent compound **14f** with the

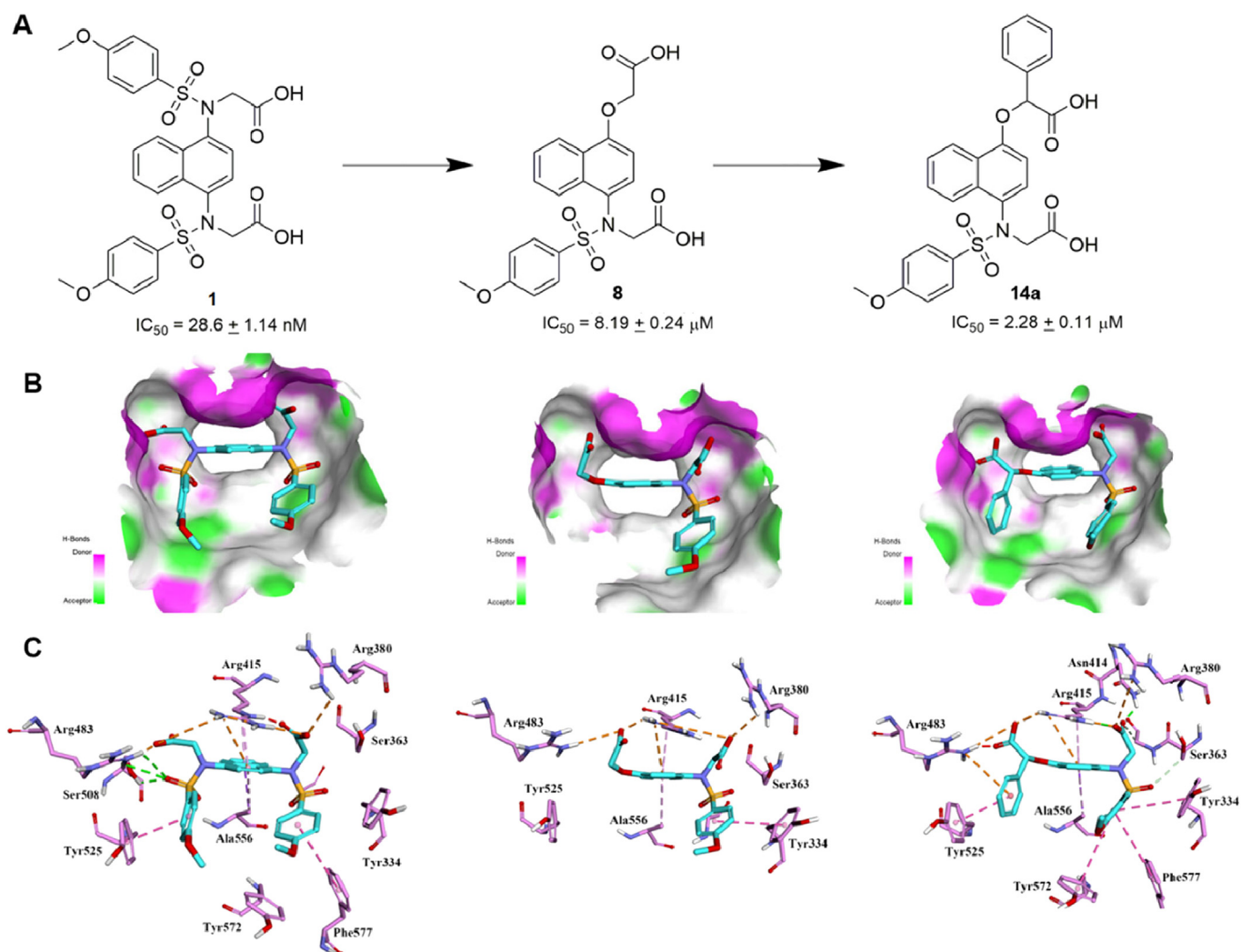


Fig. 2. Discovery of 2-oxy-2-phenylacetic acid substituted naphthalene sulfonamide derivatives. (A) The schemes of structure modification of **14a**. (B) Docked poses of **1**, **8** and **14a** with KEAP1. (C) Interaction modes of **1**, **8** and **14a** with KEAP1. Hydrogen bonds are represented by green dashed lines, the electrostatic interactions are represented by orange dashed lines, and the hydrophobic interactions are represented by pink dashed lines. The carbon atoms of small molecules and KEAP1 residues are colored cyan and purple, respectively. (For interpretation of the references to color in this figure legend, the reader is referred to the Web version of this article.)

2,4,6-trimethyl substitution, which is approximately 4-fold increased potency than that of **14a**. However, compared with our first reported small molecule inhibitor **1** ($IC_{50} = 28.6$ nM), further structure optimization of **14f** may be necessary to afford gains in potency.

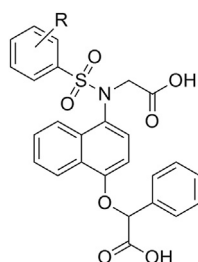
2.2.2. Substituent transformation on the benzene sulfonamide fragment in the P4 sub-pocket

The docking study showed that **14f** can form the π - π stacking interactions with Tyr525 in the P4 sub-pocket, therefore we turned our attention to the modification of the benzene acetic acid fragment in the P4 sub-pocket of this scaffold. Based on our previous study of this pocket and the docking pose of **14f**, a substituent is preferable in the para position of the phenyl ring. As shown in Fig. 3A, the benzene ring extended toward outside of the binding pocket, which closely approximated the outer solvent region. Therefore, a series of compounds (**20a**–**20j**) containing substituted benzene sulfonamide fragment were synthesized.

As shown in Table 2, it appears as though strong electron-withdrawing groups are not well tolerated at this position, as the inhibitory activity of the trifluoromethyl substituent **20a** decreased

to micromolar level ($IC_{50} = 1.19$ μ M). The trifluoromethyl group may decrease the polarization of the benzene ring, thus impairing the π - π stacking interactions with Tyr525 in the P4 sub-pocket. Comparatively, an increase in potency by the phenolic hydroxyl (**20b**, $IC_{50} = 0.16$ μ M), which is the preferred substituent in the study of peptide inhibitors, may be attributed to a hydrogen bonding interaction between the phenolic hydroxyl and Tyr525 in the P4 sub-pocket. Attractively, **20c** with the methoxyl substituent exhibited dramatic increase in PPI inhibitory activity ($IC_{50} = 0.075$ μ M), indicating that hydrophobic group is preferable in this position. Replacing the methoxyl group with the ethoxyl group diminished the activity (**20d**, $IC_{50} = 0.15$ μ M), indicating the possible steric hindrance, and it was further proved by that the isopropoxyl substituent induced the further activity decrease (**20e**, $IC_{50} = 0.50$ μ M) and the tertiary butyl substituent hugely diminished the activity (**20f**, $IC_{50} = 19$ μ M). The carboxamide group did not give good performance in activity (**20g**, $IC_{50} = 0.98$ μ M). It suggested that the hydrophilic groups may be disadvantageous in this position. Halogen substituents (**20h**–**20j**) all gave better performance than hydrogen substituent but had differences in activity: F and Cl displayed equal inhibition activity and both better than Br.

Table 1
KEAP1-NRF2 inhibitory activities and ARE induction fold results of the compounds **14a**–**14o**.^a



No.	R	IC ₅₀ ± SE (μM)	ARE induction fold					
			0.01 μM	0.1 μM	1 μM	5 μM	10 μM	20 μM
14a	4-OCH ₃	2.28 ± 0.11	1.02 ± 0.02	1.00 ± 0.14	1.12 ± 0.48	1.24 ± 0.09	1.97 ± 0.24	2.89 ± 0.14
14b	-H	17.78 ± 1.06	1.11 ± 0.55	1.12 ± 0.15	1.09 ± 0.19	1.17 ± 0.91	1.98 ± 0.12	2.21 ± 0.10
14c	4-CH ₃	2.69 ± 0.12	1.11 ± 0.07	1.03 ± 0.48	1.12 ± 0.03	1.32 ± 0.09	2.11 ± 0.08	3.11 ± 0.19
14d	4-C(CH ₃) ₃	0.98 ± 0.01	1.01 ± 0.14	1.04 ± 0.24	1.11 ± 0.01	2.38 ± 0.92	3.45 ± 1.01	4.76 ± 0.49
14e	3,4-OCH ₃	2.30 ± 0.12	1.12 ± 0.17	1.09 ± 0.11	1.08 ± 0.91	1.15 ± 0.66	2.34 ± 0.19	3.23 ± 0.27
14f	2,4,6-CH ₃	0.58 ± 0.01	1.03 ± 0.54	1.11 ± 0.15	1.34 ± 0.23	3.66 ± 1.21	4.78 ± 1.12	6.58 ± 0.18
14g	4-NHCOCH ₃	5.23 ± 1.03	1.09 ± 0.10	1.08 ± 0.77	1.01 ± 0.17	1.12 ± 0.11	1.34 ± 0.18	1.98 ± 0.31
14h	4-NO ₂	4.79 ± 1.03	1.00 ± 0.44	1.01 ± 0.03	1.02 ± 0.27	1.23 ± 0.02	1.33 ± 0.66	1.45 ± 0.51
14i	4-CONH ₂	2.69 ± 0.08	1.12 ± 0.01	1.02 ± 0.02	1.33 ± 0.04	1.33 ± 0.14	1.54 ± 0.31	2.55 ± 0.15
14j	4-CF ₃	6.66 ± 1.05	1.02 ± 0.08	1.34 ± 0.11	1.21 ± 0.12	1.17 ± 0.23	1.25 ± 1.21	2.09 ± 0.10
14k	4-OCF ₃	5.84 ± 1.01	1.01 ± 0.02	1.01 ± 0.08	1.33 ± 0.14	1.23 ± 0.08	1.14 ± 0.23	1.76 ± 0.82
14l	4-F	5.16 ± 1.11	1.13 ± 0.55	1.09 ± 0.56	1.19 ± 0.17	1.12 ± 0.34	1.45 ± 0.11	2.11 ± 1.01
14m	4-Cl	7.64 ± 1.03	1.14 ± 0.02	1.04 ± 0.19	1.09 ± 0.14	1.23 ± 0.28	1.55 ± 0.31	1.91 ± 0.34
14n	4-Br	2.97 ± 0.12	1.09 ± 0.02	1.09 ± 0.02	1.23 ± 0.40	1.11 ± 0.41	1.67 ± 0.14	2.38 ± 0.15
14o	5,6-C ₆ H ₄	0.78 ± 0.01	1.10 ± 0.19	1.13 ± 0.02	1.28 ± 0.02	3.44 ± 0.02	4.33 ± 0.12	6.11 ± 0.33

^a Values shown are the means ± SEM (n = 3).

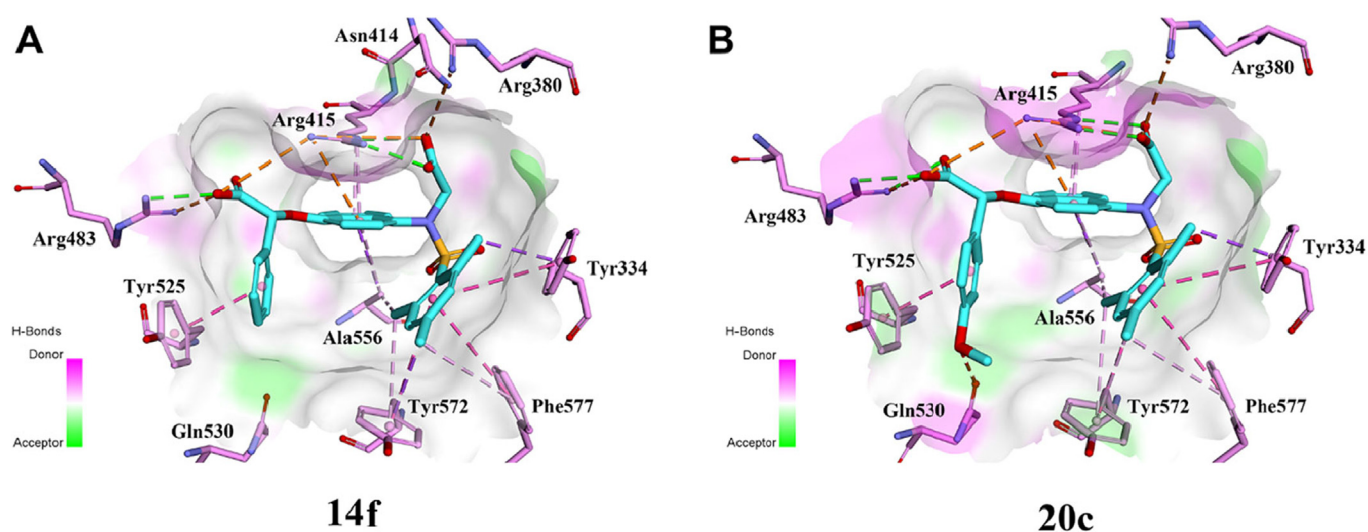


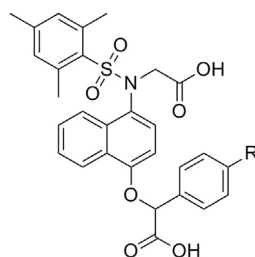
Fig. 3. Docked poses of **14f** (A) and **20c** (B) with KEAP1. Hydrogen bonds are represented by green dashed lines, the electrostatic interactions are represented by orange dashed lines, and the hydrophobic interactions are represented by pink dashed lines. The carbon atoms of small molecules and KEAP1 residues are colored cyan and purple, respectively. (For interpretation of the references to color in this figure legend, the reader is referred to the Web version of this article.)

We speculated that the weak electron-withdrawing ability of the halogen substituents might enhance the π - π stacking interactions between the phenyl ring and Tyr525 in P4. Though Br can make stronger hydrophobic interactions than F and Cl, the size of Br might be too large for this pocket to gain the superiority in activity.

Taken together, modification of the benzene acetic acid fragment afforded **20c** with stronger affinity for the P4 sub-pocket and approximately 8-fold increased PPI inhibitory activity compared to **14f**. In order to deeply understand the binding mode of our compound with KEAP1, the docking simulations

were performed to analyze the most active compound **20c** bound to KEAP1. As illustrated in Fig. 3B, compared to the template compound **14a**, introduction of the 2,4,6-trimethyl substitution increased the interactions with Tyr 334, Phe577 and Tyr572 in the P5 sub-pocket. In the exploration of the P4 sub-pocket, visual inspection of the docking poses revealed that introduction of the hydrophobic *para*-methoxyl increased the interactions with Tyr525 and probably formed a new electrostatic interaction with Gln530, which might in some extent contribute to the enhanced affinity to KEAP1.

Table 2
KEAP1-NRF2 inhibitory activities and ARE induction fold results of the compounds **20a**–**20j**.^a



No.	R	IC ₅₀ ± SE (μM)	ARE induction fold					
			0.01 μM	0.1 μM	1 μM	5 μM	10 μM	20 μM
20a	-CF ₃	1.19 ± 0.12	1.01 ± 0.14	1.00 ± 0.24	1.09 ± 0.19	2.24 ± 0.54	3.12 ± 1.12	4.28 ± 1.19
20b	-OH	0.16 ± 0.01	1.02 ± 0.55	1.11 ± 0.11	1.56 ± 0.76	4.58 ± 0.41	5.34 ± 0.54	8.29 ± 1.32
20c	-OCH ₃	0.075 ± 0.001	1.02 ± 0.43	1.23 ± 0.17	2.87 ± 0.21	5.78 ± 1.56	7.83 ± 1.98	13.38 ± 1.32
20d	-OCH ₂ CH ₃	0.15 ± 0.01	1.11 ± 0.07	1.04 ± 0.14	1.61 ± 0.05	4.24 ± 0.84	5.27 ± 1.11	8.78 ± 1.12
20e	-OCH(CH ₃) ₂	0.50 ± 0.01	1.13 ± 0.02	1.05 ± 0.28	1.24 ± 0.02	3.38 ± 0.17	4.89 ± 1.18	6.91 ± 1.14
20f	-C(CH ₃) ₃	19 ± 1.09	1.01 ± 0.02	1.02 ± 0.15	1.03 ± 0.11	1.12 ± 0.34	1.24 ± 0.01	2.13 ± 0.11
20g	-NHCOCH ₃	0.98 ± 0.01	1.00 ± 0.08	1.12 ± 0.67	1.10 ± 0.02	3.10 ± 0.11	4.08 ± 1.10	5.11 ± 0.98
20h	-F	0.17 ± 0.01	1.10 ± 0.14	1.07 ± 0.14	1.55 ± 0.02	4.48 ± 1.11	5.02 ± 0.43	8.33 ± 1.13
20i	-Cl	0.19 ± 0.01	1.04 ± 0.02	1.08 ± 0.43	1.42 ± 0.67	4.51 ± 0.64	5.99 ± 0.78	9.58 ± 1.45
20j	-Br	0.43 ± 0.01	1.00 ± 0.21	1.23 ± 0.15	1.34 ± 0.22	3.38 ± 1.10	4.89 ± 1.12	6.91 ± 0.49

^a Values shown are the means ± SEM (n = 3).

2.3. Binding characterization of **20c**

Then, the KEAP1 binding affinity and the KEAP1 binding characters of the most potent compound **20c** were investigated using both an isothermal scanning calorimetry (ITC) assay and biolayer interferometry (BLI). As shown in Fig. 4A, the ITC profile is typical of a reversible 1:1 binding stoichiometry, indicating that one **20c** molecule bound to one molecule of KEAP1 and curve-fitting analysis parameters were appropriately configured. By use of these parameters, **20c** had a K_d of 24.0 nM for KEAP1, with a strong enthalpy to binding ($\Delta H = -26.25 \text{ kcal mol}^{-1}$) and a relatively unfavorable entropic component ($T\Delta S = -15.85 \text{ kcal mol}^{-1}$), which suggested a putative enthalpy-driven process in the binding of **20c** to KEAP1. Then the BLI assay, which allows for the real time monitoring of the interactions between molecules, was carried out to measure the binding kinetics of **20c** to KEAP1. Consistent with the ITC result, the BLI experiment gave a K_d of 36.5 nM, and the dissociation curves showed that **20c** is a long-acting compound with prolonged residence time (Fig. 4B). Taken together, the above results demonstrated that **20c** can directly bind to KEAP1 *in vitro* with a strong affinity.

2.4. **20c** effectively activated NRF2-ARE regulated cytoprotective defense system

In view of the promising character of **20c**, we first investigated the cellular activities of these compounds using the ARE-luciferase reporter assay in HepG2-ARE-C8 cells. As shown in Tables 1 and 2, **20c**, which is optimal in PPI inhibition activity, gave the best performance among these compounds in the NRF2-ARE inducing activity. Therefore, it was chosen for further cell-based evaluation. Translocation of NRF2 into the nucleus is essential for the trans-activation of ARE-regulated genes. Therefore, we examined the nuclear and cytoplasmic NRF2 levels after treatment of the RAW264.7 cells with **20c**. A time response study with **20c** (10 μM) demonstrated that nuclear translocation of NRF2 began within 2 h, maximized at 8 h and subsequently declined after 16 h (Fig. 5A). We then investigated whether **20c** is potent in promoting the

transcription of NRF2-driven genes. Quantitative real-time PCR (qRT-PCR) analysis was performed to measure the mRNA levels of three selected downstream genes: *HO-1* (Heme oxygenase 1), *NQO1* (NAD(P)H: Quinone Oxidoreductase 1) and *GCLM* (glutamate-cysteine ligase, modifier subunit). As shown in Fig. 5B, after 12 h treatment, **20c** strongly increased the transcription of NRF2 regulated genes in RAW264.7 cells at a concentration-dependent manner. In a time-course study, NRF2 activation effects were observed after 4 h treatment of **20c** (10 μM) and reached the maximal effects at 16 h (Fig. 5C). Consistent with these results, western blotting experiments demonstrated that the treatment of the RAW264.7 cells with **20c** induced NRF2, HO-1, NQO-1 and GCLM protein expression in both concentration- and time-dependent manner (Fig. 5D and E).

2.5. **20c** enhanced the antioxidant capacity in macrophage RAW 264.7 cells

After the validation of high cellular NRF2 activation effects of **20c**, we then explored the effects of **20c** on antioxidant capacity of RAW 264.7 cells against cellular oxidative stress. Firstly, the effect of **20c** on the LPS induced augment of ROS level in RAW264.7 cells was detected through the living cell microscopy using the redox-sensitive fluorescent probe c-H₂DCF-DA. As shown in Fig. 6A, after treating RAW264.7 cells with 1 μg/mL LPS for 6 h, a remarkably strong living cell fluorescence microscopic signal was observed, which was resulted from the high oxidation of the incorporated c-H₂DCF-DA. Treatment with 10 μM of **20c** significantly reduced ROS generation to nearly normal level (Fig. 6A and B). Subsequently, the activities of two important antioxidant enzymes, superoxide dismutase (SOD) and glutathione peroxidase (GSH-Px), were determined. Cells were treated with LPS (1 μg/mL) alone or in combination with different concentrations (1, 10 μM) of **20c**. LPS exposure induced sharp decrease in the activities of SOD and GSH-Px, while the thereafter treatment with 10 μM of **20c** notably restored the SOD and GSH-Px levels (Fig. 6C and D), indicating the restoration of the antioxidant capacity of RAW 264.7 cells. The ratio of reduced glutathione (GSH) to oxidized glutathione (GSSG),

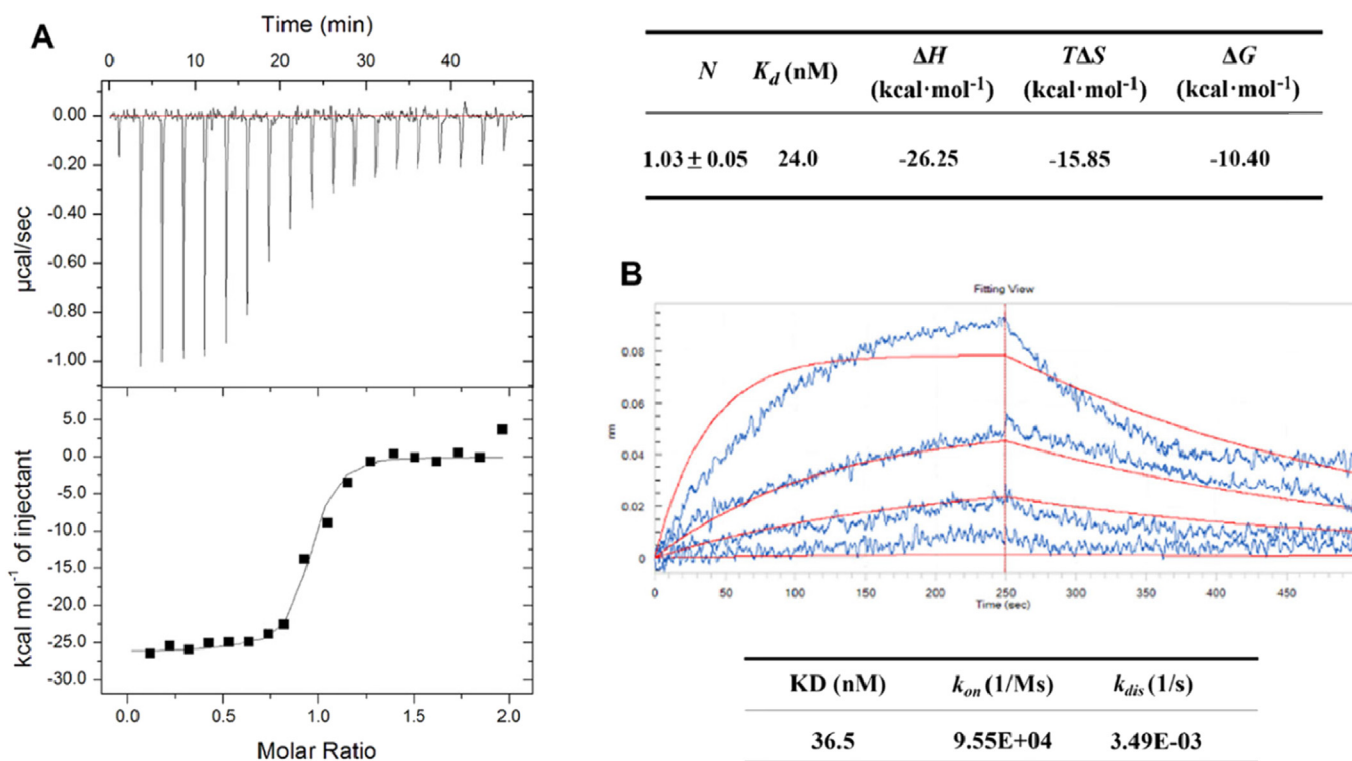


Fig. 4. Compound **20c** exhibited tight KEAP1 binding *in vitro*. (A) ITC profile of the titration of the KEAP1 Kelch domain with **20c**. Calculated values are stoichiometry (N), affinity (K_d), enthalpy change (ΔH), and entropy change (ΔS). Total Gibbs free energy (ΔG) is calculated according to the equation $\Delta G = \Delta H - T\Delta S$, with T the temperature set up for the ITC experiment. (B) BLI concentration-response curves reflecting the direct binding of **20c** to KEAP1. Concentrations: 250 nM, 50 nM, 20 nM, 1 nM.

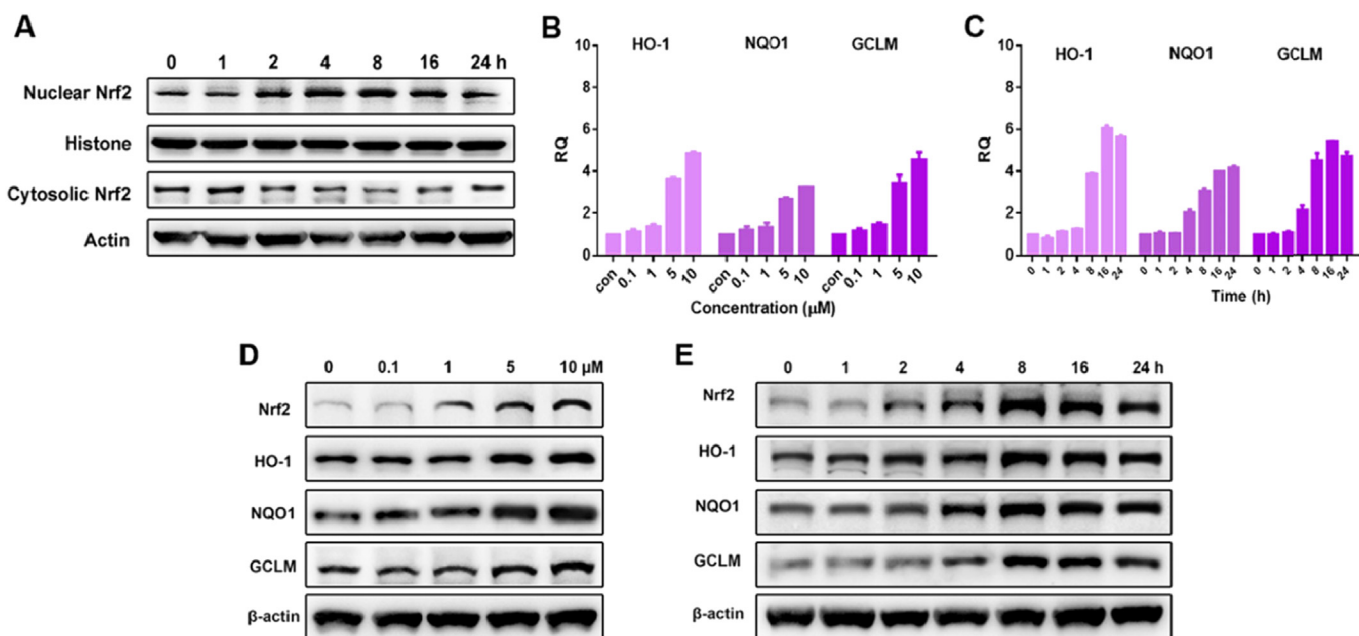


Fig. 5. **20c** activated NRF2-ARE regulated cytoprotective defense system. (A) Effect of **20c** on the nuclear translocation of the NRF2 protein ($n = 3$ independent observations). (B) Expression of NRF2-regulated genes after treatment with **20c** in RAW264.7 cells. The mRNA levels of NRF2-targeted genes were measured at 12 h after treatment of RAW264.7 cells with various concentrations of **20c**. (C) The mRNA levels of NRF2-targeted genes were measured at various time points after treatment with 10 μ M **20c**. Values shown are the means \pm SEM ($n = 3$). *** $P < 0.001$, ** $P < 0.01$, and * $P < 0.05$, which were calculated with one-way ANOVA. (D) Expression of NRF2-regulated proteins after treatment with **20c** in RAW264.7 cells. The protein levels of NRF2 and its downstream proteins were measured at 12 h after treatment of RAW264.7 cells with various concentrations of **20c** ($n = 3$ independent observations). (E) The protein levels of NRF2 and its downstream proteins were measured at various time points after treatment with 10 μ M **20c** ($n = 3$ independent observations).

which is interpreted as evidence of redox balance and reducing power, and the oxidative-related marker, myeloperoxidase (MPO) activity, were also assessed (Fig. 6E and F). LPS treatment induced the concomitant decline in the ratio of GSH to GSSG, while treatment with **20c** at the concentration of 10 μM almost restored the ratio back to normal. As expected, treatment with **20c** also showed a concentration-dependent reversal in LPS-induced increase of MPO activity. These results clearly demonstrated that **20c** enhanced the capacity of the antioxidant system in the RAW264.7 cells under inflammatory conditions.

2.6. **20c** attenuates LPS-induced production of inflammation factors in RAW 264.7 cells

Following activation by inflammatory stimuli such as LPS, macrophages secrete various inflammatory mediators such as interleukin-1 β (IL-1 β), IL-6, tumor necrosis factor α (TNF- α) and nitric oxide (NO). Activation of NRF2 has been proven to be effective on relieving inflammatory conditions. Therefore, we investigated whether **20c** can alleviate LPS induced inflammatory conditions in mouse RAW264.7 cells. As shown in Fig. 7A–D, LPS exposure resulted in sharp rise of the levels of the inflammatory factors IL-1 β , IL-6, TNF- α and NO in RAW264.7 cells. However, this expression was markedly attenuated in macrophages by treatment with **20c** in a concentration-dependent manner, and treatment with **20c** at the high concentration (10 μM) almost reduced these cytokines to the basal level.

2.7. **20c** reduced the LPS-induced production of the pro-inflammatory factors in vivo

After confirming the cellular NRF2 activation effects of **20c**, we finally investigated the *in vivo* curative effect of **20c**. To explore the suitability of **20c** for *in vivo* administration, the ADME properties and pharmacokinetics of **20c** were evaluated. As shown in Table 3, **20c** was relatively stable in co-incubation with rat liver microsomes with half-life of 10.5 h, indicating high metabolic stability. Moreover, it was observed that **20c** has no CYP inhibition on 1A2, 2C9, 2C19, 2D6 and 3A4 when tested at 10 μM . Then we evaluated the pharmacokinetics of **20c** for IV. **20c** showed appropriate overall pharmacokinetic profile in rats as 1 mg/kg IV dosing led to half-life of 1.72 ± 0.42 h.

Finally, the *in vivo* therapeutic effect of **20c** in LPS-induced inflammation mouse model was also evaluated. Female C57BL/6 mice (20 ± 2 g) were treated with LPS (300 $\mu\text{g}/\text{kg}$, IP) and 4 h later received an IP injection (500 μL) containing the desired dose of **20c** for 3 days. The control group only received saline (IP, 500 μL) during the whole experiment. As a positive control, another group received dexamethasone (DXM), which is the widely used steroid anti-inflammatory drug. As shown in Fig. 8A–D, LPS administration resulted in the markedly elevation of the inflammatory cytokines including interferon- γ (IFN- γ), IL-1 β , IL-6 and TNF- α in the model group. In contrast, administration of **20c** diminished inflammatory response, showing comparable therapeutic effects with DXM at the same dose (10 mg/kg). Noteworthy, a significant dose-effect relationship was observed as **20c** at high dose (10 mg/kg) showed much more potent anti-inflammatory activities. These results

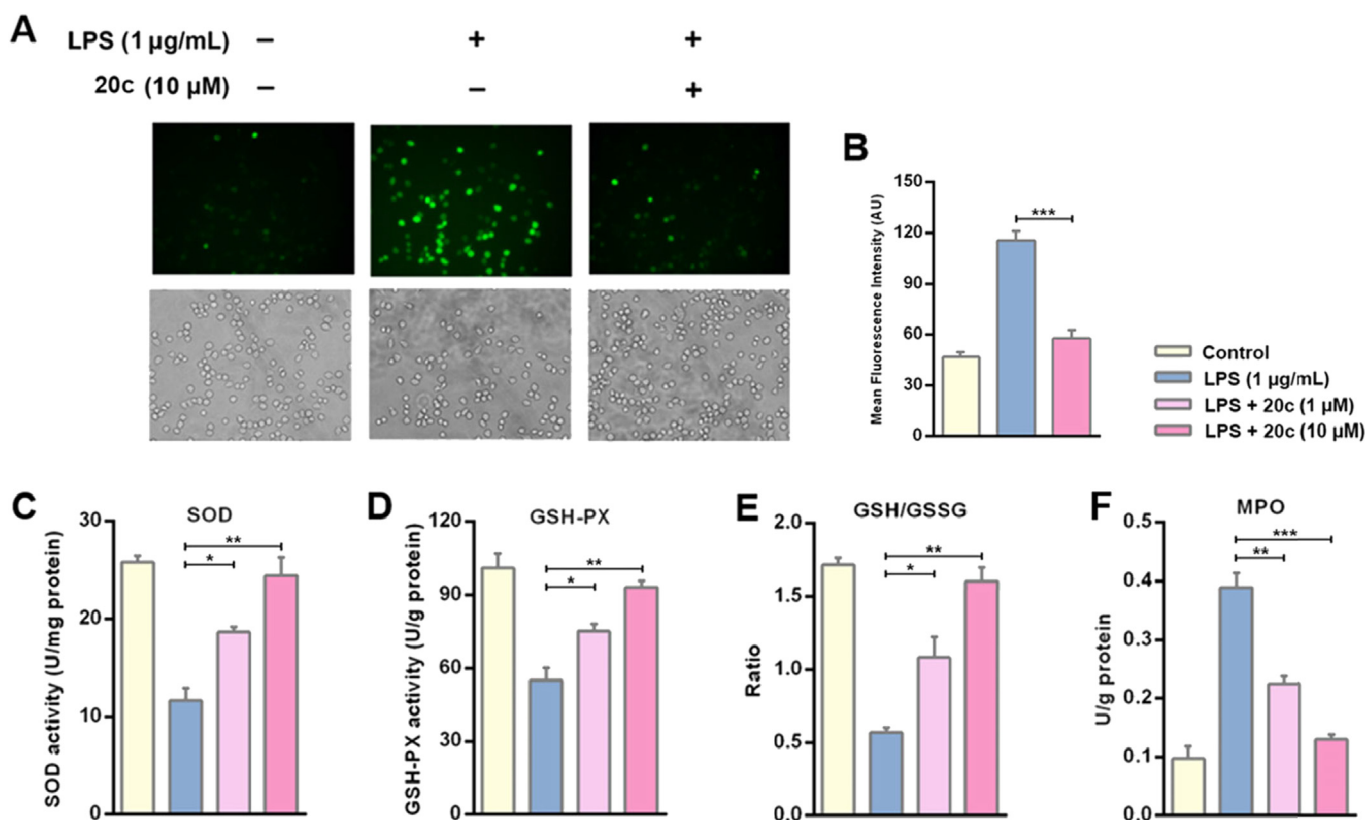


Fig. 6. **20c** increased the expression of the antioxidant enzymes SOD (C) and GSH-PX (D), the ratio of GSH/GSSG (E) and scavenged ROS (A) and MPO (F) induced by LPS in mouse RAW 264.7 cells. (B) Mean fluorescence intensity analysis of ROS level in mouse RAW 264.7 cells analyzed by ImageJ v1.8.0. The RAW 264.7 cells were pretreated with LPS (1 $\mu\text{g}/\text{mL}$) for 6 h, and then treated with **20c** for another 12 h. The results are expressed as the means \pm SEM ($n = 3$ independent observations). * $p < 0.05$, ** $p < 0.01$, *** $p < 0.001$, which were calculated with one-way ANOVA.

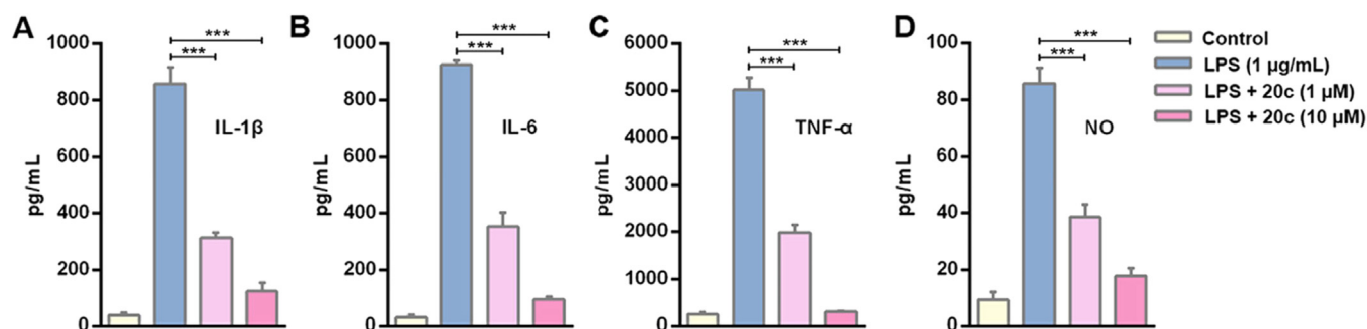


Fig. 7. Quantification of the inflammatory cytokines IL-1 β (A), IL-6 (B), TNF- α (C) activities and NO production (D) in mouse RAW 264.7 cells. The RAW 264.7 cells were pretreated with LPS (1 μ g/mL) for 6 h, and then treated with **20c** for another 12 h. The concentration of the above inflammatory cytokines secreted in the culture media was measured by Elisa kits. The results are expressed as the means \pm SEM (n = 3 independent observations). ***p < 0.001, which were calculated with one-way ANOVA.

indicated that the small molecule KEAP1-NRF2 inhibitor **20c** had profound therapeutic effect on oxidative stress related inflammatory conditions *in vivo*.

2.8. Chemistry

The synthesis of compound **14a-o** are shown in Scheme 1. Peroxidation of commercially available 1-nitronaphthalene afforded 4-nitro-1-naphthol (**9**). The nitro group of **9** was reduced by hydrogen and Pd/C, and the subsequent *N*-Boc protection of the amino group gave compound **10**. Using the conventional Williamson ether synthesis, compound **11** was then prepared. Deprotection of the *N*-Boc and the subsequent condensation with arylsulfonyl chloride gave compounds **12a-o**, respectively. Compounds **13a-o** were obtained by nucleophilic substitution of NH by bromoacetate in the presence of K₂CO₃ in DMF. Hydrolysis of the ester groups of compounds **13a-o** yielded the target compounds **14a-o**.

The synthesis of compound **20c, d, h-j** are shown in Scheme 2. The reaction of compounds **15c, d, h-j** with *N*-bromosuccinimide (NBS) in the presence of 2,2-Azobisisobutyronitrile (AIBN) as a catalyst gave compounds **16c, d, h-j**, and the subsequent Williamson ether synthesis with compound **10** obtained compounds **17c, d, h-j**. Deprotection of the *N*-Boc and the subsequent condensation with 2-Mesitylenesulfonyl chloride gave compounds **18c, d, h-j**, respectively. Compounds **19a-e** were obtained by nucleophilic substitution of NH by bromoacetate in the presence of K₂CO₃ in DMF. Hydrolysis of the ester groups of compounds **19c, d, h-j** yielded the target compounds **20c, d, h-j**.

The synthesis of compound **20a, b, e-g** are shown in Scheme 3. The *O*-Bn protection of the hydroxyl group in compound **10** resulted in compound **21**. Deprotection of the *N*-Boc in compound **21** and subsequent condensation with 2-Mesitylenesulfonyl chloride gave

compound **22**. Compound **23** was obtained by nucleophilic substitution of NH by bromoacetate in the presence of K₂CO₃ in DMF. Deprotection of the benzyl group with Pd/C in THF solution produced compound **24**. The reaction of compounds **15a, b, e-g** with NBS in the presence of AIBN as a catalyst gave compounds **16a, b, e-g**, and the subsequent Williamson ether synthesis with compound **24** obtained compounds **19a, b, e-g**. Hydrolysis of the ester groups of compounds **19a, b, e-g** yielded the target compounds **20a, b, e-g**.

3. Conclusion

The transcription factor NRF2 allows adaptation and survival under stressed conditions via regulating the gene expression of diverse networks of cytoprotective proteins. Modulation of NRF2 activation by directly disrupting KEAP1-NRF2 PPI has emerged as a rational strategy to discover preventive and therapeutic agents for diseases involving oxidative stress and inflammation. Recent years have seen a surge in interest in the development of KEAP1-NRF2 PPI inhibitors with a 1,4-diaminonaphthalene core. In this study, a series of 2-oxy-2-phenylacetic acid substituted naphthalene sulfonamide derivatives were rationally designed and synthesized as potent KEAP1-NRF2 inhibitors and the 1,4-diaminonaphthalene substituted pattern has been identified as unnecessary for inhibiting KEAP1-NRF2 interaction.

On the basis of the potent KEAP1-NRF2 PPI inhibitor **1** reported by our group previously, we introduced the oxyacetic acid group to substitute one of the *N*-acetic acid substituted sulfonamide group. We suggested that the preferred oxyacetic acid group may occupy the P1 sub-pocket of KEAP1 and a series of compounds containing the oxyacetic acid group were synthesized and evaluated. The acetic acid group and the core naphthalene ring, which are the key features for KEAP1 binding, have been retained, and the structure-

Table 3
Detailed *in vitro/in vivo* profile for **20c**.^a

Rat liver microsomes					
T _{1/2} (hr)	Cl _{int} (<i>in vitro</i>) (μ L/min/mg)	ER	CL _H (mL/min/kg)	Cl _{int} (<i>in vivo</i>) (mL/min/kg)	
10.5	1.57	4.89%	2.69	2.83	
CYP inhibition IC ₅₀ (μ M)					
CYP1A2	CYP2C9	CYP2C19	CYP2D6	CYP3A4	
>10	>10	>10	>10	>10	
Rat Pharmacokinetic properties (1 mg/kg i.v. Dosing)					
AUC _{0-t} (ng·hr/mL)	AUC _{0-∞} (ng·hr/mL)	CL _F (mL/min/kg)	T _{1/2} (hr)	C _{max} (ng/mL)	V _{Z,F} (mL/kg)
2546 \pm 348	2649 \pm 401	6.38 \pm 1.01	1.72 \pm 0.42	15100 \pm 2326	953 \pm 290

^a The data were measured in triplicates.

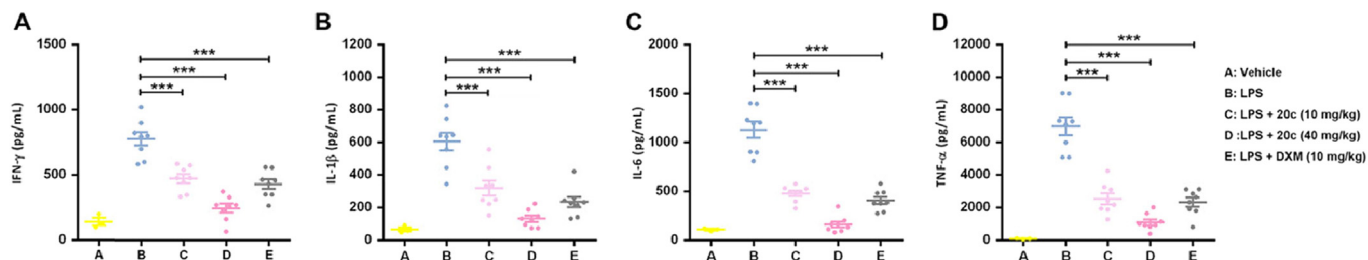
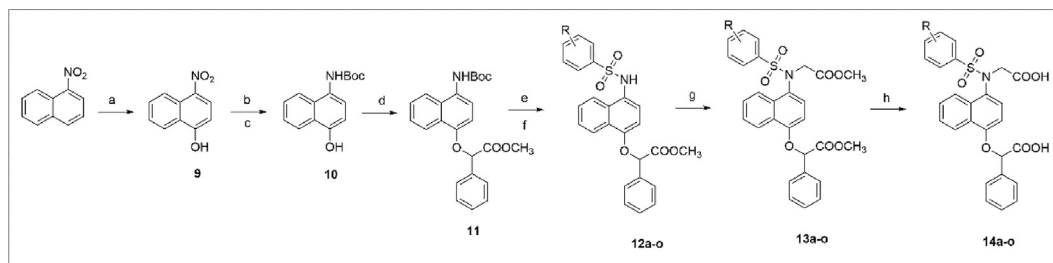
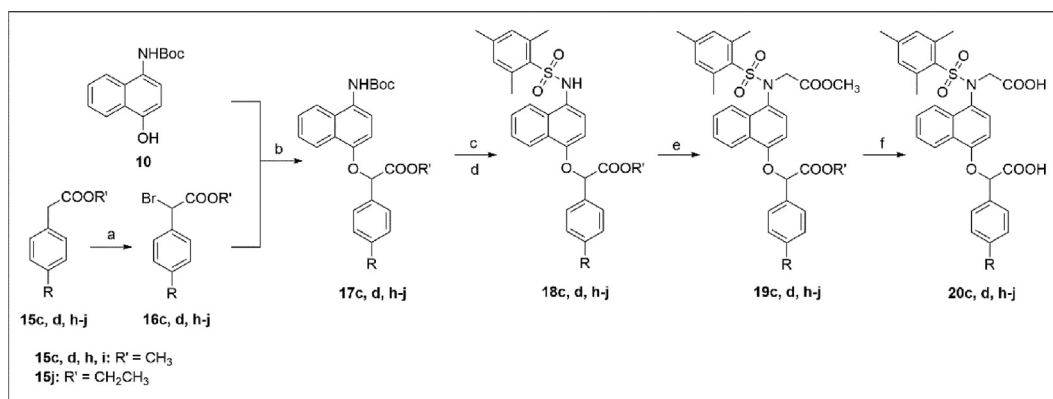


Fig. 8. 20c reduced the LPS-induced production of the pro-inflammatory factors *in vivo*. Levels of serum IFN- γ (A), IL-1 β (B), IL-6 (C) and TNF- α (D) and were measured by Elisa kits. Mice were randomly divided into five groups: control group (n = 3), LPS group (300 μ g/kg, n = 8), LPS + 20c (10 mg/kg) group (n = 8), LPS + 20c (40 mg/kg) group (n = 8), LPS + DXM (10 mg/kg) group (n = 8). ***p < 0.001, which were calculated with one-way ANOVA.



Scheme 1. Synthesis of target compounds 14a-o.

^aConditions and reagents: (a) (CH₃)₃COOH, KOH, DMSO/H₂O, r. t. 4 h, yield 82%; (b) H₂, Pd/C, MeOH, 6 h; (c) (Boc)₂O, TEA, MeOH, 5 h, yield 83%; (d) methyl 2-bromo-2-phenylacetate, K₂CO₃, DMF, r. t. 2 h, yield 46%; (e) CF₃COOH, CH₂Cl₂, r. t. 30 min; (f) substituted arylsulfonyl chloride, pyridine, THF, r. t. 10 h, yield 50–70%; (g) BrCH₂COOCH₃, K₂CO₃, DMF, 2 h, yield 80–85%; (h) LiOH, MeOH/H₂O, 10 h, yield 85–90%.



Scheme 2. Synthesis of target compounds 20c, d, h-j.

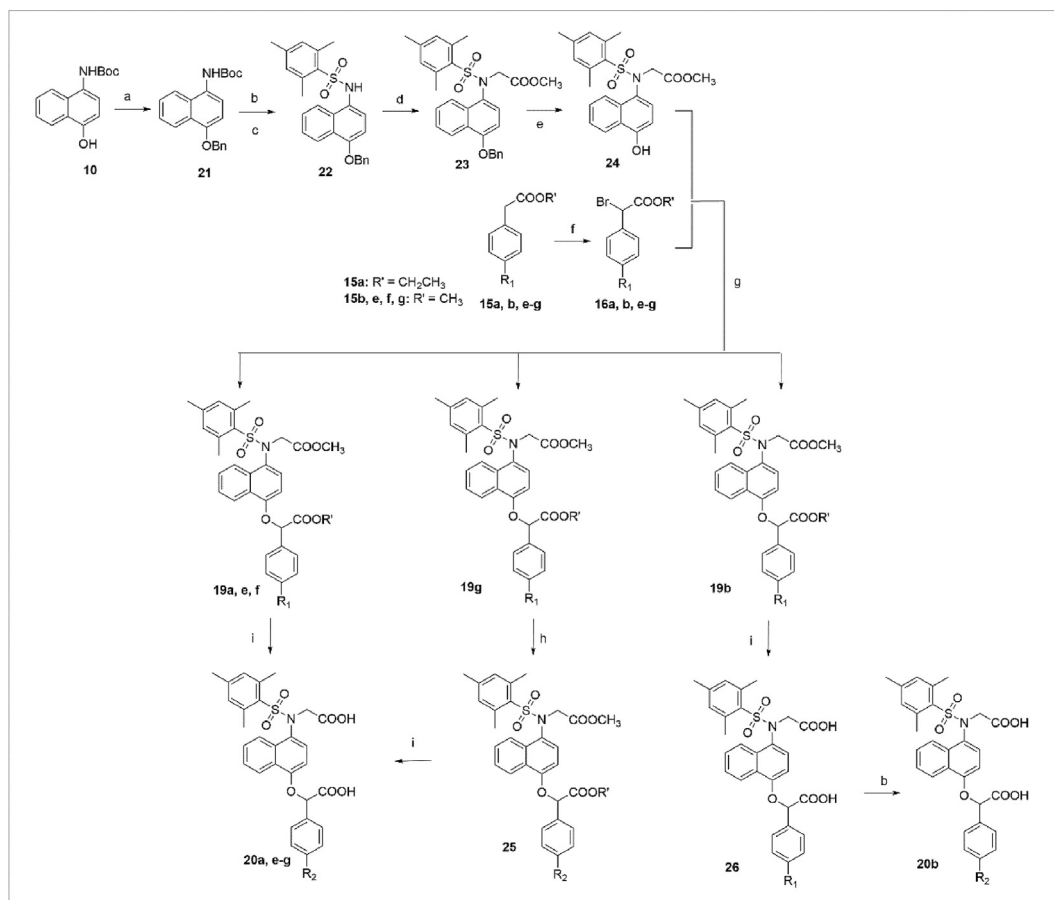
^aConditions and reagents: (a) NBS, AIBN, CHCl₃, 60 °C, yield 70–80%; (b) K₂CO₃, DMF, r. t. 2 h, yield 46%; (c) CF₃COOH, CH₂Cl₂, r. t. 30 min; (d) 2-Mesitylenesulfonyl chloride, pyridine, THF, r. t. 10 h, yield 50–70%; (e) BrCH₂COOCH₃, K₂CO₃, DMF, 2 h, yield 80–85%; (f) LiOH, MeOH/H₂O, 10 h, yield 85–90%.

activity and structure-property relationships of the substitutions in the P4 and P5 sub-pockets have been investigated. Intensive structural modifications led to the identification of **20c** as the most potent KEAP1-NRF2 PPI inhibitor with an IC₅₀ of 75 nM in the FP competition assay. As revealed by the binding mode analysis, **20c** is likely to fulfill all the five sub-pockets of KEAP1; the oxyacetic acid group in the P1 sub-pocket could retain the original strong polar interactions; the 2,4,6-trimethyl substitution increased the hydrophobic interactions in the P5 sub-pocket; the hydrophobic *para*-methoxyl increased the interactions with Tyr525 and probably formed a new polar interaction with Gln530 in the P4 sub-pocket and the other part of the molecule could interact with KEAP1 in a similar way as the lead compound **1**.

The subsequent binding characterization assays demonstrated that **20c** had strong binding affinity with a K_d of 24 nM for KEAP1

and prolonged residence time with KEAP1. Cell-based experiments showed that the KEAP1-NRF2 PPI inhibitor **20c** can activate the NRF2-ARE pathway and induce the expression of Nrf2 downstream cytoprotective genes and proteins in macrophage cells. **20c** can also enhance the antioxidant capacity in macrophage RAW 264.7 cells and therefore antagonized the LPS induced cellular inflammatory conditions. Encouraged by the above results, the *in vivo* evaluation was carried out to further confirm the anti-inflammatory effects of **20c** in the LPS-induced inflammation mouse model. The decrease of the LPS induced circulating inflammatory markers, including IFN- γ , IL-1 β , IL-6 and TNF- α proved that **20c** could effectively relieve the LPS induced inflammatory responses.

In this study, we identified the 2-oxy-2-phenylacetic acid substituted naphthalene sulfonamide derivative, **20c**, as a potent KEAP1-NRF2 inhibitor and proved the therapeutic potential of



Scheme 3. Synthesis of target compounds **20a, b, e-g**.

^aConditions and reagents: (a) PhCH₂Br, K₂CO₃, DMF, r. t. yield 46%; (b) CF₃COOH, CH₂Cl₂, r. t. 30 min; (c) 2-Mesitylenesulfonyl chloride, pyridine, THF, r. t. 10 h, yield 75%; (d) BrCH₂COOCH₃, K₂CO₃, DMF, r. t. 2 h, yield 90%; (e) H₂, Pd/C, THF, 60 °C, yield 95%; (f) NBS, AIBN, CHCl₄, 60 °C, yield 70–80%; (g) K₂CO₃, DMF, r. t. yield 50–60%; (h) CF₃COOH, CH₂Cl₂, r. t. 1 h; acetic anhydride, TEA, r. t. 5 h; (i) LiOH, MeOH/H₂O, r. t. 10 h, yield 90–95%.

KEAP1-NRF2 inhibitor in LPS induced inflammatory conditions. Our study provided a new chemical probe with which to further study the biology of the KEAP1-NRF2-ARE pathway and demonstrated that activation of NRF2 by small molecule KEAP1-NRF2 PPI inhibitors could be a viable way to antagonize stress and inflammation related disorders.

4. Experimental section

4.1. Chemical synthesis for all target compounds

4.1.1. 2-((4-(N-(carboxymethyl)-4-methoxyphenylsulfonamido)naphthalen-1-yl)oxy)-2-phenylacetic acid (**14a**)

To a solution of **13a** (61.0 mg, 111.0 μmol) in MeOH/H₂O (3 mL/3 mL) was added LiOH·H₂O (300.0 mg, 12.5 mmol). After 10 h stirring at room temperature, the reaction mixture was then diluted in 30 mL water and quenched with 2 M hydrochloric acid to pH 4. The crude product was obtained through filtration. Recrystallization from ethyl acetate/n-hexane gave compound **14a** as a white solid, yield 53.4%, m. p. 128.5–130.5 °C. ¹H NMR (300 MHz, DMSO-*d*₆) δ: 3.83–3.85 (m, 3H), 4.23–4.47 (m, 2H), 6.05 (s, 1H), 6.81–6.84 (m, 1H), 7.02–7.12 (m, 3H), 7.38–7.70 (m, 9H), 8.00–8.06 (m, 1H), 8.27–8.30 (m, 1H) 13.07 (br, 2H); IR (KBr, cm⁻¹): 3464, 1736, 1340, 1263, 1154; HRMS (ESI): found 522.1225 (C₂₇H₂₄NO₈S, [M+H]⁺, requires 522.1217); HPLC (85:15 methanol: water with 1% TFA): t_R = 4.2 min, 96.8%.

4.1.2. 2-((4-(N-(carboxymethyl)phenylsulfonamido)naphthalen-1-yl)oxy)-2-phenylacetic acid (**14b**)

The same procedure as **14a**, white solid, yield 76.6%, m. p. 160.0–162.5 °C. ¹H NMR (300 MHz, DMSO-*d*₆) δ: 4.25–4.36 (m, 1H), 4.48–4.56 (m, 1H), 6.08–6.09 (m, 1H), 6.82–6.85 (m, 1H), 7.12–7.15 (m, 1H), 7.39–7.69 (m, 12H), 7.92–7.97 (m, 1H), 8.29–8.32 (m, 1H), 12.93 (br, 2H); IR (KBr, cm⁻¹): 3467, 1732, 1596, 1350, 1163, 1091; EI-MS HRMS (ESI): found 492.1109 (C₂₆H₂₂NO₇S, [M+H]⁺, requires 492.1111); HPLC (85:15 methanol: water with 1% TFA): t_R = 4.1 min, 98.6%.

4.1.3. 2-((4-(N-(carboxymethyl)-4-methylphenylsulfonamido)naphthalen-1-yl)oxy)-2-phenylacetic acid (**14c**)

The same procedure as **14a**, gray solid, yield 73.2%, m. p. 179.8–181.3 °C. ¹H NMR (300 MHz, DMSO-*d*₆) δ: 2.27 (s, 3H), 4.25–4.50 (m, 2H), 6.08–6.09 (m, 1H), 6.82–6.84 (m, 1H), 7.09–7.11 (m, 1H), 7.32–7.55 (m, 9H), 7.64–7.70 (m, 2H), 7.99–8.05 (m, 1H), 8.29–8.30 (m, 1H), 12.87–13.21 (m, 2H); IR (KBr, cm⁻¹): 3468, 1735, 1340, 1234, 1155; HRMS (ESI): found 506.1278 (C₂₇H₂₄NO₇S, [M+H]⁺, requires 506.1268); HPLC (85:15 methanol: water with 1% TFA): t_R = 4.37, 4.42 min, 96.7%.

4.1.4. 2-((4-(4-(tert-butyl)-N-(carboxymethyl)phenylsulfonamido)naphthalen-1-yl)oxy)-2-phenylacetic acid (**14d**)

The same procedure as **14a**, gray solid, yield 89.0%, m. p. 101.7–103.3 °C. ¹H NMR (300 MHz, DMSO-*d*₆) δ: 1.30–1.32 (m, 9H),

4.20–4.32 (m, 1H), 4.48–4.56 (m, 1H), 6.12–6.13 (m, 1H), 6.87–6.89 (m, 1H), 7.19–7.23 (m, 1H), 7.44–7.70 (m, 9H), 7.72–7.79 (m, 2H), 7.81–7.87 (m, 1H), 8.29–8.32 (m, 1H), 12.98 (br, 2H); IR (KBr, cm^{-1}): 3442, 1735, 1390, 1348, 1163; EI-MS HRMS (ESI): found 548.1743 ($\text{C}_{30}\text{H}_{30}\text{NO}_7\text{S}$, $[\text{M}+\text{H}]^+$ requires 548.1737); HPLC (85:15 methanol: water with 1% TFA): $t_{\text{R}} = 5.9$ min, 95.6%.

4.1.5. 2-((4-(*N*-(carboxymethyl)-3,4-dimethoxyphenylsulfonamido)naphthalen-1-yl)oxy)-2-phenylacetic acid (**14e**)

The same procedure as **14a**, gray solid, yield 78.9%, m. p. 68.7–71.1 °C. ^1H NMR (300 MHz, CDCl_3) δ 3.67 (s, 3H), 3.92 (s, 3H), 4.10–4.16 (m, 1H), 5.05–5.11 (m, 1H), 5.74 (s, 1H), 6.59–6.62 (m, 1H), 6.82–6.85 (m, 1H), 7.13–7.19 (m, 2H), 7.30–7.37 (m, 1H), 7.49–7.64 (m, 5H), 7.66–7.73 (m, 3H), 8.38–8.40 (m, 1H); IR (KBr, cm^{-1}): 3415, 1734, 1508, 1390, 1332, 1264, 1154; EI-MS HRMS (ESI): found 552.1331 ($\text{C}_{28}\text{H}_{26}\text{NO}_9\text{S}$, $[\text{M}+\text{H}]^+$ requires 552.1323); HPLC (85:15 methanol: water with 1% TFA): $t_{\text{R}} = 3.8, 3.9$ min, 98.8%.

4.1.6. 2-((4-(*N*-(carboxymethyl)-2,4,6-trimethylphenylsulfonamido)naphthalen-1-yl)oxy)-2-phenylacetic acid (**14f**)

The same procedure as **14a**, white solid, yield 76.9%, m. p. 144.6–146.9 °C. ^1H NMR (300 MHz, $\text{DMSO}-d_6$) δ : 2.12–2.20 (m, 9H), 4.28–4.38 (m, 1H), 4.64–4.72 (m, 1H), 6.11–6.14 (m, 1H), 6.83–6.89 (m, 3H), 7.42–7.48 (m, 5H), 7.62–7.79 (m, 4H), 8.27–8.29 (m, 1H), 12.88 (br, 2H); ^{13}C NMR (75 MHz, $\text{DMSO}-d_6$) δ : 20.29, 22.88, 53.08, 78.16, 105.48, 122.08, 122.92, 125.48, 126.71, 127.11, 127.61, 128.37, 130.30, 131.58, 131.80, 133.30, 136.73, 139.11, 141.93, 153.05, 170.40, 170.54, 170.72, 170.92; IR (KBr, cm^{-1}): 3415, 1729, 1389, 1328, 1235, 1156; EI-MS HRMS (ESI): found 534.1569 ($\text{C}_{29}\text{H}_{27}\text{NO}_7\text{S}$, $[\text{M}+\text{H}]^+$ requires 534.1581); HPLC (85:15 methanol: water with 1% TFA): $t_{\text{R}} = 5.8$ min, 96.2%.

4.1.7. 2-((4-(4-acetamido-*N*-(carboxymethyl)phenylsulfonamido)naphthalen-1-yl)oxy)-2-phenylacetic acid (**14g**)

The same procedure as **14a**, white gray solid, yield 73.9%, m. p. 68.6–71.0 °C. ^1H NMR (300 MHz, $\text{DMSO}-d_6$) δ : 2.10 (s, 3H), 4.25–4.49 (m, 2H), 6.08–6.09 (m, 1H), 6.82–6.85 (m, 1H), 7.09–7.11 (m, 1H), 7.42–7.76 (m, 11H), 8.02–8.05 (m, 1H), 8.28–8.29 (m, 1H), 10.37 (s, 1H), 12.83–13.31 (m, 2H); IR (KBr, cm^{-1}): 3412, 1735, 1591, 1330, 1263, 1156; HRMS (ESI): found 571.1170 ($\text{C}_{28}\text{H}_{24}\text{N}_2\text{NaO}_8\text{S}$, $[\text{M}+\text{Na}]^+$ requires 571.1146); HPLC (85:15 methanol: water with 1% TFA): $t_{\text{R}} = 3.5, 3.8$ min, 97.7%.

4.1.8. 2-((4-(*N*-(carboxymethyl)-4-nitrophenylsulfonamido)naphthalen-1-yl)oxy)-2-phenylacetic acid (**14h**)

The same procedure as **14a**, gray solid, yield 56.0%, m. p. 179.0–180.9 °C. ^1H NMR (300 MHz, $\text{DMSO}-d_6$) δ : 4.28–4.37 (m, 1H), 4.59–4.66 (m, 1H), 6.07 (s, 1H), 6.82–6.86 (m, 1H), 7.18–7.21 (m, 1H), 7.41–7.48 (m, 3H), 7.55–7.58 (m, 2H), 7.64–7.70 (m, 2H), 7.89–7.97 (m, 3H), 8.32–8.38 (m, 3H), 13.23 (br, 2H); HRMS (ESI): found 554.1239 ($\text{C}_{26}\text{H}_{24}\text{N}_3\text{O}_9\text{S}$, $[\text{M} + \text{NH}_4]^+$ requires 554.1228); IR (KBr, cm^{-1}): 3425, 1719, 1352, 1235, 1167; HPLC (85:15 methanol: water with 1% TFA): $t_{\text{R}} = 4.4, 4.6$ min, 97.1%.

4.1.9. 2-((4-(4-carbamoyl-*N*-(carboxymethyl)phenylsulfonamido)naphthalen-1-yl)oxy)-2-phenylacetic acid (**14i**)

The same procedure as **14a**, white purple solid, yield 74.1%, m. p. 179.2–180.9 °C. ^1H NMR (300 MHz, $\text{DMSO}-d_6$) δ : 4.32–4.38 (m, 1H), 4.52–4.60 (m, 1H), 6.06–6.07 (m, 1H), 6.83–6.86 (m, 1H), 7.14–7.17 (m, 1H), 7.38–7.59 (m, 4H), 7.64–7.81 (m, 4H), 7.81–8.09 (m, 3H), 8.20–8.28 (m, 1H), 8.30–8.32 (m, 1H); IR (KBr, cm^{-1}): 3489, 1754, 1685, 1353, 1168, 1125; EI-MS HRMS (ESI): found 535.1168 ($\text{C}_{27}\text{H}_{22}\text{N}_2\text{O}_8\text{S}$, $[\text{M}+\text{H}]^+$ requires 535.1170); HPLC (85:15 methanol: water with 1% TFA): $t_{\text{R}} = 3.6$ min, 95.2%.

4.1.10. 2-((4-(*N*-(carboxymethyl)-4-(trifluoromethyl)phenylsulfonamido)naphthalen-1-yl)oxy)-2-phenylacetic acid (**14j**)

The same procedure as **14a**, white solid, yield 84.4%, m. p. 166.7–168.9 °C. ^1H NMR (300 MHz, $\text{DMSO}-d_6$) δ : 4.24–4.36 (m, 1H), 4.58–4.65 (m, 1H), 6.08 (s, 1H), 6.85–6.87 (m, 1H), 7.20–7.23 (m, 1H), 7.36–7.58 (m, 5H), 7.63–7.69 (m, 2H), 7.83–7.95 (m, 5H), 8.28–8.32 (m, 1H), 13.12 (br, 2H); IR (KBr, cm^{-1}): 3475, 1729, 1352, 1323, 1167, 1130; EI-MS HRMS (ESI): found 582.0809 ($\text{C}_{27}\text{H}_{20}\text{F}_3\text{NNaO}_7\text{S}$, $[\text{M}+\text{Na}]^+$ requires 582.0805); HPLC (85:15 methanol: water with 1% TFA): $t_{\text{R}} = 5.0$ min, 96.2%.

4.1.11. 2-((4-(*N*-(carboxymethyl)-4-(trifluoromethoxy)phenylsulfonamido)naphthalen-1-yl)oxy)-2-phenylacetic acid (**14k**)

The same procedure as **14a**, white solid, yield 71.7%, m. p. 215.0–216.8 °C. ^1H NMR (300 MHz, $\text{DMSO}-d_6$) δ : 4.24–4.35 (m, 1H), 4.59–4.66 (m, 1H), 6.10–6.11 (m, 1H), 6.87–6.90 (m, 1H), 7.25–7.28 (m, 1H), 7.37–7.59 (m, 7H), 7.65–7.72 (m, 2H), 7.77–7.88 (m, 3H), 8.26–8.37 (m, 1H), 13.10–13.16 (m, 2H); IR (KBr, cm^{-1}): 3416, 1736, 1595, 1350, 1260, 1162; HRMS (ESI): found 598.0778 ($\text{C}_{27}\text{H}_{20}\text{F}_3\text{NNaO}_8\text{S}$, $[\text{M}+\text{Na}]^+$ requires 598.0754); HPLC (85:15 methanol: water with 1% TFA): $t_{\text{R}} = 5.3$ min, 96.9%.

4.1.12. 2-((4-(*N*-(carboxymethyl)-4-fluorophenylsulfonamido)naphthalen-1-yl)oxy)-2-phenylacetic acid (**14l**)

The same procedure as **14a**, white solid, yield 81.5%, m. p. 97.1–99.3 °C. ^1H NMR (300 MHz, $\text{DMSO}-d_6$) δ : 4.25–4.35 (m, 1H), 4.50–4.58 (m, 1H), 6.07 (s, 1H), 6.83–6.86 (m, 1H), 7.15–7.18 (m, 1H), 7.37–7.73 (m, 11H), 7.92–7.95 (m, 1H), 8.28–8.29 (m, 1H), 12.96 (br, 2H); IR (KBr, cm^{-1}): 3466, 1731, 1390, 1237, 1155; HRMS (ESI): found 527.1295 ($\text{C}_{26}\text{H}_{24}\text{FN}_2\text{O}_7\text{S}$, $[\text{M} + \text{NH}_4]^+$ requires 527.1283); HPLC (85:15 methanol: water with 1% TFA): $t_{\text{R}} = 4.3$ min, 96.6%.

4.1.13. 2-((4-(*N*-(carboxymethyl)-4-chlorophenylsulfonamido)naphthalen-1-yl)oxy)-2-phenylacetic acid (**14m**)

The same procedure as **14a**, white gray solid, yield 69.4%, m. p. 190.1–192.5 °C. ^1H NMR (300 MHz, $\text{DMSO}-d_6$) δ : 4.25–4.36 (m, 1H), 4.52–4.59 (m, 1H), 6.08 (s, 1H), 6.85 (d, 1H, $J = 8.49$ Hz), 7.18 (d, 1H, $J = 8.10$ Hz), 7.38–7.71 (m, 11H), 7.94–8.00 (m, 1H), 8.29–8.30 (m, 1H), 12.8–13.4 (br, 2H); IR (KBr, cm^{-1}): 3467, 1735, 1343, 1235, 1157; HRMS (ESI): found 526.0714 ($\text{C}_{26}\text{H}_{21}\text{ClNO}_7\text{S}$, $[\text{M}+\text{H}]^+$ requires 526.0722); HPLC (85:15 methanol: water with 1% TFA): $t_{\text{R}} = 4.9$ min, 96.9%.

4.1.14. 2-((4-(4-bromo-*N*-(carboxymethyl)phenylsulfonamido)naphthalen-1-yl)oxy)-2-phenylacetic acid (**14n**)

The same procedure as **14a**, white gray solid, yield 63.3%, m. p. 180.0–182.3 °C. ^1H NMR (300 MHz, $\text{DMSO}-d_6$) δ : 4.22–4.33 (m, 1H), 4.49–4.56 (m, 1H), 6.05 (s, 1H), 6.83 (d, 1H, $J = 8.49$ Hz), 7.15 (d, 1H, $J = 8.19$ Hz), 7.36–7.70 (m, 11H), 7.93–7.98 (m, 1H), 8.27–8.28 (m, 1H); IR (KBr, cm^{-1}): 3475, 1736, 1343, 1235, 1101; HRMS (ESI): found 570.0215 ($\text{C}_{26}\text{H}_{21}\text{BrNO}_7\text{S}$, $[\text{M}+\text{H}]^+$ requires 570.0217); HPLC (85:15 methanol: water with 1% TFA): $t_{\text{R}} = 5.1$ min, 96.1%.

4.1.15. 2-((4-(*N*-(carboxymethyl)naphthalene-2-sulfonamido)naphthalen-1-yl)oxy)-2-phenylacetic acid (**14o**)

The same procedure as **14a**, white solid, yield 92.0%, m. p. 190.5–193.0 °C. ^1H NMR (300 MHz, $\text{DMSO}-d_6$) δ : 4.34–4.45 (m, 1H), 4.53–4.61 (m, 1H), 6.06–6.08 (m, 1H), 6.78–6.82 (m, 1H), 7.12–7.14 (m, 1H), 7.38–7.55 (m, 5H), 7.63–7.76 (m, 5H), 8.05–8.13 (m, 4H), 8.32–8.37 (m, 2H), 12.83 (br, 2H); IR (KBr, cm^{-1}): 3442, 1730, 1593, 1342, 1153, 1131; EI-MS HRMS (ESI): found 542.1282 ($\text{C}_{30}\text{H}_{24}\text{NO}_7\text{S}$, $[\text{M}+\text{H}]^+$ requires 542.1268); HPLC (85:15 methanol: water with 1% TFA): $t_{\text{R}} = 4.9$ min, 97.6%.

4.1.16. 2-((4-(*N*-(carboxymethyl)-2,4,6-trimethylphenylsulfonamido)naphthalen-1-yl)oxy)-2-(4-(trifluoromethyl)phenyl)acetic acid (**20a**)

The same procedure as **14a**, white solid, yield 58.2%, m. p. >250 °C. ¹H NMR (300 MHz, CDCl₃) δ: 2.11–2.19 (m, 9H), 4.10–4.16 (m, 1H), 5.15–5.21 (m, 1H), 5.71 (s, 1H), 6.48–6.51 (m, 1H), 6.68 (s, 2H), 7.37–7.39 (m, 3H), 7.45–7.49 (m, 1H), 7.67–7.69 (m, 2H), 7.80–7.82 (m, 2H), 8.23–8.26 (m, 1H); IR (KBr, cm⁻¹): 3416, 1735, 1637, 1326, 1122, 1068; EI-MS HRMS (ESI): found 624.1268 (C₃₀H₂₆F₃NNaO₇S, [M+Na]⁺ requires 624.1274); HPLC (85:15 methanol: water with 1% TFA): t_R = 7.0 min, 95.1%.

4.1.17. 2-((4-(*N*-(carboxymethyl)-2,4,6-trimethylphenylsulfonamido)naphthalen-1-yl)oxy)-2-(4-hydroxyphenyl)acetic acid (**20b**)

To a solution of compound **26** (300.0 mg, 443.0 μmol) in CH₂Cl₂ (5.0 mL), CF₃COOH (165.0 μL, 2.2 mmol) was added, and the reaction mixture was stirred for 0.5 h at r. t. After the completion of the reaction monitored by TLC, saturated Na₂CO₃ was added to the reaction mixture until pH 7. Then the reaction mixture was extracted with EtOAc (× 3). The combined organic extracts were washed with saturated NaHCO₃ solution, H₂O and saturated NaCl solution, then dried over Na₂SO₄, filtered, and concentrated in vacuo. Purification by silica gel column chromatography provided compound **20b** as a white solid, yield 30.9%, m. p. >250 °C. ¹H NMR (300 MHz, DMSO-*d*₆) δ: 2.16–2.21 (m, 9H), 4.15–4.20 (m, 1H), 4.61–4.67 (m, 1H), 5.70–5.77 (m, 1H), 6.72–6.81 (m, 3H), 6.84–6.87 (m, 2H), 7.36–7.50 (m, 5H), 7.72–7.77 (m, 1H), 8.18–8.23 (m, 1H); IR (KBr, cm⁻¹): 3415, 1638, 1618, 1154, 1122; EI-MS HRMS (ESI): found 550.1513 (C₂₉H₂₈NO₈S, [M+H]⁺ requires 550.1530); HPLC (85:15 methanol: water with 1% TFA): t_R = 4.0 min, 95.5%.

4.1.18. 2-((4-(*N*-(carboxymethyl)-2,4,6-trimethylphenylsulfonamido)naphthalen-1-yl)oxy)-2-(4-methoxyphenyl)acetic acid (**20c**)

The same procedure as **14a**, gray solid, yield 78.0%, m. p. 145.1–147.8 °C. ¹H NMR (300 MHz, DMSO-*d*₆) δ: 2.12–2.19 (m, 9H), 3.75–3.77 (m, 3H), 4.26–4.36 (m, 1H), 4.64–4.71 (m, 1H), 6.02–6.05 (m, 1H), 6.83–6.91 (m, 3H), 6.94–7.02 (m, 2H), 7.37–7.50 (m, 3H), 7.55–7.58 (m, 2H), 7.71–7.78 (m, 1H), 8.23–8.24 (m, 1H), 12.86–13.20 (m, 2H); ¹³C NMR (75 MHz, DMSO-*d*₆) δ: 25.03, 27.61, 27.67, 57.63, 59.82, 59.86, 81.71, 110.35, 110.50, 118.78, 118.83, 126.77, 127.65, 127.78, 130.34, 130.40, 131.58, 132.53, 132.61, 132.63, 132.66, 133.42, 133.44, 134.92, 136.35, 136.39, 136.60, 136.64, 137.87, 137.96, 143.93, 143.97, 146.81, 146.84, 157.56, 164.36, 175.02, 175.05, 175.45, 175.50; IR (KBr, cm⁻¹): 3415, 1734, 1512, 1240, 1122; EI-MS HRMS (ESI): found 586.1519 (C₃₀H₂₉NNaO₈S, [M+Na]⁺ requires 586.1506); HPLC (85:15 methanol: water with 1% TFA): t_R = 5.4 min, 97.3%.

4.1.19. 2-((4-(*N*-(carboxymethyl)-2,4,6-trimethylphenylsulfonamido)naphthalen-1-yl)oxy)-2-(4-ethoxyphenyl)acetic acid (**20d**)

The same procedure as **14a**, gray solid, yield 35.7%, m. p. 127.8–130.7 °C. ¹H NMR (300 MHz, CDCl₃) δ: 1.45 (t, 3H, *J* = 6.99 Hz), 2.20–2.27 (m, 9H), 4.08 (q, 2H, *J* = 6.99 Hz), 4.19–4.25 (m, 1H), 5.24–5.30 (m, 1H), 5.65 (s, 1H), 6.53–6.56 (m, 1H), 6.76 (s, 2H), 6.98–7.01 (m, 2H), 7.38–7.45 (m, 3H), 7.58–7.64 (m, 3H), 8.30–8.33 (m, 1H); IR (KBr, cm⁻¹): 3421, 1740, 1513, 1306, 1254, 1159; EI-MS HRMS (ESI): found 600.1652 (C₃₁H₃₁NNaO₈S, [M+Na]⁺ requires 600.1663); HPLC (85:15 methanol: water with 1% TFA): t_R = 6.4 min, 96.1%.

4.1.20. 2-((4-(*N*-(carboxymethyl)-2,4,6-trimethylphenylsulfonamido)naphthalen-1-yl)oxy)-2-(4-isopropoxyphenyl)acetic acid (**20e**)

The same procedure as **14a**, gray solid, yield 44.1%, m. p. 115.6–118.0 °C. ¹H NMR (300 MHz, CDCl₃) δ: 1.39–1.41 (m, 6H), 2.23 (s, 3H), 2.30 (s, 6H), 4.21–4.27 (m, 1H), 4.60–4.68 (m, 1H), 5.28–5.33 (m, 1H), 5.68 (s, 1H), 6.56–6.59 (m, 1H), 6.79 (s, 2H), 7.00–7.03 (m, 2H), 7.44–7.46 (m, 3H), 7.61–7.67 (m, 3H), 8.34–8.37 (m, 1H); IR (KBr, cm⁻¹): 3449, 1736, 1492, 1331, 1259, 1156; EI-MS HRMS (ESI): found 592.2009 (C₃₂H₃₄NO₈S, [M+H]⁺ requires 592.2000); HPLC (85:15 methanol: water with 1% TFA): t_R = 10.5 min, 95.1%.

4.1.21. 2-(4-(*tert*-butyl)phenyl)-2-((4-(*N*-(carboxymethyl)-2,4,6-trimethylphenyl sulfonamido) naphthalen-1-yl)oxy)acetic acid (**20f**)

The same procedure as **14a**, yellow solid, yield 24.5%, m. p. 190.2–192.6 °C. ¹H NMR (300 MHz, CDCl₃) δ: 1.37 (s, 9H), 2.21–2.27 (m, 9H), 4.20–4.26 (m, 1H), 5.27–5.34 (m, 1H), 5.70 (s, 1H), 6.54–6.56 (m, 1H), 6.77 (s, 2H), 7.38–7.54 (m, 3H), 7.51–7.54 (m, 2H), 7.60–7.63 (m, 1H), 7.67–7.69 (m, 2H), 8.35–8.37 (m, 1H); IR (KBr, cm⁻¹): 3420, 1735, 1638, 1324, 1157, 1093; EI-MS HRMS (ESI): found 590.2202 (C₃₃H₃₆NO₇S, [M+H]⁺ requires 590.2207); HPLC (85:15 methanol: water with 1% TFA): t_R = 10.6 min, 94.9%.

4.1.22. 2-(4-(acetamidophenyl)-2-((4-(*N*-(carboxymethyl)-2,4,6-trimethylphenyl sulfonamido) naphthalen-1-yl)oxy)acetic acid (**20g**)

The same procedure as **14a**, light yellow solid, yield 37.3%, m. p. 214.0–216.5 °C. ¹H NMR (300 MHz, DMSO-*d*₆) δ: 2.03–2.05 (m, 3H), 2.11 (s, 3H), 2.16–2.19 (m, 6H), 4.26–4.37 (m, 1H), 5.63–5.70 (m, 1H), 5.99–6.01 (m, 1H), 6.83–6.88 (m, 3H), 7.36–7.42 (m, 2H), 7.47–7.57 (m, 1H), 7.60–7.65 (m, 2H), 7.72–7.80 (m, 2H), 8.24–8.28 (m, 1H), 8.31–8.35 (m, 1H), 10.03–10.07 (s, 1H), 13.12 (br, 2H); IR (KBr, cm⁻¹): 3416, 1603, 1515, 1318, 1155, 1090; EI-MS HRMS (ESI): found 613.1604 (C₃₁H₃₀N₂O₈S, [M+Na]⁺ requires 613.1615); HPLC (85:15 methanol: water with 1% TFA): t_R = 4.0, 4.1 min, 97.8%.

4.1.23. 2-((4-(*N*-(carboxymethyl)-2,4,6-trimethylphenylsulfonamido)naphthalen-1-yl)oxy)-2-(4-fluorophenyl)acetic acid (**20h**)

The same procedure as **14a**, gray solid, yield 71.8%, m. p. 152.3–155.0 °C. ¹H NMR (300 MHz, CDCl₃) δ: 2.22 (s, 3H), 2.29 (s, 6H), 4.21–4.27 (m, 1H), 5.27–5.33 (m, 1H), 5.73 (s, 1H), 6.56–6.59 (m, 1H), 6.78 (s, 2H), 7.18–7.24 (m, 2H), 7.45–7.48 (m, 3H), 7.59–7.62 (m, 1H), 7.73–7.78 (m, 2H), 8.31–8.35 (m, 1H); IR (KBr, cm⁻¹): 3464, 1762, 1508, 1333, 1270, 1153; EI-MS HRMS (ESI): found 574.1304 (C₂₉H₂₆FNNaO₇S, [M+Na]⁺ requires 574.1306); HPLC (85:15 methanol: water with 1% TFA): t_R = 5.8 min, 96.7%.

4.1.24. 2-((4-(*N*-(carboxymethyl)-2,4,6-trimethylphenylsulfonamido)naphthalen-1-yl)oxy)-2-(4-chlorophenyl)acetic acid (**20i**)

The same procedure as **14a**, gray solid, yield 40.7%, m. p. 169.1–171.3 °C. ¹H NMR (300 MHz, CDCl₃) δ: 2.20 (s, 3H), 2.28 (s, 6H), 4.20–4.26 (m, 1H), 5.26–5.32 (m, 1H), 5.71 (s, 1H), 6.55–6.58 (m, 1H), 6.77 (s, 2H), 7.45–7.49 (m, 5H), 7.59–7.61 (m, 1H), 7.68–7.71 (m, 2H), 8.31–8.33 (m, 1H), 8.57 (br, 2H); IR (KBr, cm⁻¹): 2983, 1763, 1685, 1334, 1159, 1131; EI-MS HRMS (ESI): found 590.1000 (C₂₉H₂₆ClNNaO₇S, [M+Na]⁺ requires 590.1011); HPLC (85:15 methanol: water with 1% TFA): t_R = 7.2 min, 95.5%.

4.1.25. 2-(4-(bromophenyl)-2-((4-(*N*-(carboxymethyl)-2,4,6-trimethylphenylsulfonamido)naphthalen-1-yl)oxy)acetic acid (**20j**)

The same procedure as **14a**, gray solid, yield 40.5%, m. p. 114.7–117.1 °C. ¹H NMR (300 MHz, CDCl₃) δ: 2.21 (s, 3H), 2.29 (s,

6H), 4.20–4.26 (m, 1H), 5.25–5.31 (m, 1H), 5.70 (s, 1H), 6.55–6.58 (m, 1H), 6.78 (s, 2H), 7.41–7.50 (m, 3H), 7.60–7.64 (m, 5H), 8.31–8.34 (m, 1H); IR (KBr, cm^{-1}): 3415, 1735, 1327, 1235, 1156; EI-MS HRMS (ESI): found 612.0705 ($\text{C}_{29}\text{H}_{27}\text{BrNO}_7\text{S}$, requires $[\text{M}+\text{H}]^+$ requires 612.0686); HPLC (85:15 methanol: water with 1% TFA): $t_{\text{R}} = 7.9$ min, 95.4%.

4.2. Biology

4.2.1. ITC assay

ITC was performed at 25 °C using a MicroCal ITC200 system. The sample cell was loaded with 200 μL of purified Keap1 Kelch domain at 0.005 mM in 10 mM HEPES buffer (pH 7.4). The syringe was filled with purified compound in the same buffer solution. 2 μL aliquots of 0.05 mM compound were injected 19 times with 2.5 min intervals and a stirring speed of 750 rpm into the sample cell. Data were analyzed with the MicroCal Origin software, version 7.0.

4.2.2. BLI assay

The KEAP1 Kelch domain protein was biotinylated and dissolved in a buffer of 20 mM HEPES, pH 7.0. The interaction between the inhibitor and the KEAP1 protein was determined by biolayer interferometry using an Octet Red 96 instrument (FortéBio Inc.). The binding data were collected at 30 °C. The association and dissociation plot and kinetic constants were obtained with FortéBio data analysis software.

4.2.2.1. S6. Cell culture and ARE-luciferase activity assay. HepG2 cells stably transfected with a luciferase reporter (HepG2-ARE-C8) were kindly provided by Professor Dr. A. N. Tony Kong (Rutgers University, Piscataway, NJ) and Prof. Rong Hu (China Pharmaceutical University, Nanjing). The mouse RAW 264.7 cell line was obtained from Cell Bank of Shanghai Institute of Biochemistry and Cell Biology, Shanghai Institutes for Biological Sciences, Chinese Academy of Sciences. The cells were maintained by regular passage in modified RPMI-1640 medium (GiBco, Invitrogen Corp. USA) supplied with 10% FBS, 100 units per mL penicillin and 100 $\mu\text{g}/\text{mL}$ streptomycin, cultured at 37 °C in a water vapour saturated atmosphere with 5% CO_2 .

The ARE-luciferase activity assay experimental procedures were carried out as reported previously [62].

4.2.3. Western blot analysis

Anti-NRF2 (ab62352) was purchased from Abcam (Abcam, UK). Anti-HO-1 (#5853S) were bought from Cell Signaling Technology (USA). Anti-NQO1 (sc-271116) and anti-GCLM (sc-22755) antibodies were purchased from Santa Cruz Biotechnology (Santa Cruz, CA, USA). Anti-KEAP1 antibody (10503-2-AP) was bought from Proteintech Group, Inc. Anti- β -action (AP0060) was purchased from Bioworld (Bioworld, USA). Isolation of cell fractions and Western blotting were performed as previously reported [53].

4.2.4. RNA extraction and qRT-PCR analysis

Detailed procedure of qRT-PCR was previously reported [62]. The analysis of *HO-1*, *NQO1* and *GCLM* were performed by using the StepOne System Fast Real Time PCR system (Applied Biosystems). Values are expressed as the fold of the control.

4.2.5. Detection of ROS levels

Mouse RAW 264.7 cells were seeded in 6-well plates at the density of 70–80% confluence per well for overnight incubation. Then the cells were treated with compound for indicated time. After treatment, cells were washed once with 2 mL of 10% PBS and stained with 10 μM $\text{cH}_2\text{DCF-DA}$ (S0033, Reactive Oxygen Species Assay Kit, Beyotime, China) in the dark at 37 °C for 20 min in 1640

medium free with FBS. Analysis was done with a fluorescence microscope (OLYMPUS DP72, Japan) equipped with a U-RFL-T power supply.

4.2.6. Detection of SOD, GSH-Px and MPO activities and GSH/GSSG ratio

The RAW 264.7 cells were pretreated with LPS (1 $\mu\text{g}/\text{mL}$) for 6 h, and then treated with compound for another 12 h. The activities of SOD (Total Superoxide Dismutase Assay Kit with WST-8, S0101, Beyotime, China), GSH-Px (Total Glutathione Peroxidase Assay Kit, S0058, Beyotime, China) and MPO (MPO Detection Kit, A044, Nanjing Jiancheng Bioengineering, China) and the ratio of GSH/GSSG (GSH and GSSG Assay Kit, S0053, Beyotime, China) were determined using the corresponding detection kits according to the manufacturer's instructions.

4.2.7. IL-1 β , IL-6, TNF- α , NO and IFN- γ production

Levels of IL-1 β (IL-1 β (m) ELISA kit, EK0394, Boster), IL-6 (IL-6 (m) ELISA kit, EK0411, Boster), TNF- α (TNF- α (m) ELISA kit, EK0527, Boster), NO production (Nitrate/Nitrite Assay Kit, S0023, Beyotime, China) and IFN- γ (IFN- γ (m) ELISA kit, EK0375, Boster) were evaluated using commercially available kits according to the manufacturer's instructions.

4.3. In vitro/in vivo profile assays

4.3.1. Microsome stability

The *in vitro* microsome stability of the compound was evaluated in isolated liver microsomes (from CD-1 male rat). Clozapine was used as reference compound. A solution of liver microsomes (20 mg/mL) was added to a microcentrifuge tube containing of PBS at 37 °C, and the mixture was shaken for 10 min before the actual assay was started. Then, a DMSO solution of test compound (0.1 mM) was added. For 0 min, add ice-cold acetonitrile to the wells of 0 min plate and then add NADPH stock solution (10 mM). Pre-incubate all other plates at 37 °C for 5 min. Add NADPH stock solution (10 mM) to the plates to start the reaction and timing. At 5 min, 15 min, 30 min, and 45 min, add ice-cold acetonitrile to the wells of corresponding plates, respectively, to stop the reaction. After quenching, shake the plates at the vibrator for 10 min and then centrifuge at 4000 rpm for 20 min. Transfer the supernatant from each well into a 96-well sample plate containing ultra pure water for LC-MS/MS analysis.

4.3.2. CYP inhibition assay

The *in vitro* microsome stability of the compound was evaluated in isolated human liver microsomes (Xenotech). The inhibitors of 1A2, 2C9, 2C19, 2D6 and 3A4 were 7-ethoxycoumarin, Sulfaphenazole, Omeprazole, Promethazine and Fluconazole, respectively. 150 μL of liver microsome solution/well and 2 μL of 1 mM inhibitor solution/well were added to a 96 well plate and mixed. The plate was pre-incubated in water bath at 37 °C for 10 min. Following the pre-incubation period, the reaction was initiated with the addition of 50 μL of NADPH/Substrate working solution to the samples and then mixed and incubated at 37 °C for indicated times. After that, 200 μL stop solution was added to the samples to quench the reaction. The reaction mixture was then centrifuged at 4000 rpm for 20 min at 4 °C. While centrifuging, a new 96-well plate with 300 $\mu\text{L}/\text{well}$ 50% acetonitrile was loaded. Transfer the supernatant from each well into a 96-well sample plate to bioanalytical services for LC-MS/MS analysis.

4.3.3. In vivo pharmacokinetic assay

Animals: 6 male SD rats, weight 180–220 g. Compound solutions were prepared by dissolving them in normal saline by

cosolvent before experiment. For the IV study, test compound (1 mg/kg) was administered by intravenous injection to animals. Blood samples were collected at 0.0833, 0.25, 0.5, 0.75, 1, 1.5, 2, 4, 8, 12, 24 h for the IV group. Blood samples will be put on ice until centrifuged to obtain plasma sample. The samples were then centrifuged at 4 °C at 2000 rpm for 10 min. Plasma samples were transferred and stored at approximately –80 °C prior to analysis. The plasma samples were determined by LC-MS/MS assays.

4.4. Animal experiment

The female C57BL/6 mice (body weight of 20 ± 2 g) were reared in a pathogen-free setting at 22 °C and 60% humidity for 2 days before the experiments. Mice were given free access to food and water throughout the experimental cycle. Animal experiments were approved by and performed according to guidelines established by Institutional Animal Care and Use Committee of China Pharmaceutical University.

Mice were injected with LPS (300 µg/kg, IP) and 4 h later injected intraperitoneally with the desired dose of **20c** (500 µL) for 3 days. The control group only received saline (IP) during the whole experiment. As a positive control, another group received DXM (IP, 500 µL). Animals were sacrificed 24 h after the last dose of compound and sera were collected for the measurement of inflammatory factors.

Author contributions

Qi-Dong You and Zheng-Yu Jiang conceived and designed the study. Meng-Chen Lu performed most of the biological experiment, analyzed the data and wrote the draft. Hong-Li Shao and Tian Liu synthesized the compounds. Zheng-Yu Jiang revised the manuscript extensively and submitted the manuscript on behalf of other authors. Qi-Dong You also revised this manuscript. Qi-Dong You and Zheng-Yu Jiang provided the financial support for this project. All the authors approved the final version of the manuscript.

Declaration of competing interest

The authors declare that they have no known competing financial interests or personal relationships that could have appeared to influence the work reported in this paper.

Acknowledgments

This study was supported by Projects 81773639, 81773581, 81803363 and 81930100 of the National Natural Science Foundation of China; National Science & Technology Major Project 'Key New Drug Creation and Manufacturing Program', China (No: 2018ZX09711002 and 2017ZX09302003); the Priority Academic Program Development of Jiangsu Higher Education Institutions; China Postdoctoral Science Foundation-funded Project (2017M620231 and 2018T110576); CPU2018GY02 of Double First Class Innovation Team of China Pharmaceutical University; the Project Program of State Key Laboratory of Natural Medicines, China Pharmaceutical University (No.SKLNZZ202003); Program for Outstanding Scientific and Technological Innovation Team and Jiangsu Qing Lan Project and the Young Elite Scientists Sponsorship Program by CAST.

Appendix A. Supplementary data

Supplementary data to this article can be found online at <https://doi.org/10.1016/j.ejmech.2020.112734>.

References

- [1] H. Sies, C. Berndt, D.P. Jones, Oxidative stress, *Annu. Rev. Biochem.* 86 (2017) 715–748.
- [2] L. Zhang, X. Wang, R. Cueto, C. Effi, Y. Zhang, H. Tan, X. Qin, Y. Ji, X. Yang, H. Wang, Biochemical basis and metabolic interplay of redox regulation, *Redox Biol* 26 (2019) 101284.
- [3] B.W.L. Lee, P. Ghode, D.S.T. Ong, Redox regulation of cell state and fate, *Redox Biol* 25 (2019) 101056.
- [4] A. Boutten, D. Goven, E. Artaud-Macari, J. Boczkowski, M. Bonay, NRF2 targeting: a promising therapeutic strategy in chronic obstructive pulmonary disease, *Trends Mol. Med.* 17 (2011) 363–371.
- [5] T. Suzuki, H. Motohashi, M. Yamamoto, Toward clinical application of the Keap1–Nrf2 pathway, *Trends Pharmacol. Sci.* 34 (2013) 340–346.
- [6] S. Magesh, Y. Chen, L. Hu, Small molecule modulators of keap1-nrf2-ARE pathway as potential preventive and therapeutic agents, *Med. Res. Rev.* 32 (2012) 687–726.
- [7] A. Raghunath, K. Sundarraj, R. Nagarajan, F. Arfuso, J. Bian, A.P. Kumar, G. Sethi, E. Perumal, Antioxidant response elements: discovery, classes, regulation and potential applications, *Redox Biol* 17 (2018) 297–314.
- [8] E.H. Kobayashi, T. Suzuki, R. Funayama, T. Nagashima, M. Hayashi, H. Sekine, N. Tanaka, T. Moriguchi, H. Motohashi, K. Nakayama, M. Yamamoto, Nrf2 suppresses macrophage inflammatory response by blocking proinflammatory cytokine transcription, *Nat. Commun.* 7 (2016) 11624.
- [9] J. Frijhoff, P.G. Winyard, N. Zarkovic, S.S. Davies, R. Stocker, D. Cheng, A.R. Knight, E.L. Taylor, J. Oettrich, T. Ruskovska, A.C. Gasparovic, A. Cuadrado, D. Weber, H.E. Poulsen, T. Grune, H.H. Schmidt, P. Ghezzi, Clinical relevance of biomarkers of oxidative stress, *Antioxidants Redox Signal.* 23 (2015) 1144–1170.
- [10] F. Sivandzade, S. Prasad, A. Bhalerao, L. Cucullo, NRF2 and NF- κ B interplay in cerebrovascular and neurodegenerative disorders: molecular mechanisms and possible therapeutic approaches, *Redox Biol* 21 (2019) 101059.
- [11] G.H. Liu, J. Qu, X. Shen, NF- κ B/p65 antagonizes Nrf2-ARE pathway by depriving CBP from Nrf2 and facilitating recruitment of HDAC3 to MafK, *Biochim. Biophys. Acta* 1783 (2008) 713–727.
- [12] N. Wakabayashi, S.L. Slocum, J.J. Skoko, S. Shin, T.W. Kensler, When NRF2 talks, who's listening? *Antioxidants Redox Signal.* 13 (2010) 1649–1663.
- [13] I. Bellezza, A. Tucci, F. Galli, S. Grottelli, A.L. Mierla, F. Pilioli, A. Minelli, Inhibition of NF- κ B nuclear translocation via HO-1 activation underlies alpha-tocopheryl succinate toxicity, *J. Nutr. Biochem.* 23 (2012) 1583–1591.
- [14] V. Ganesh Yerra, G. Negi, S.S. Sharma, A. Kumar, Potential therapeutic effects of the simultaneous targeting of the Nrf2 and NF- κ B pathways in diabetic neuropathy, *Redox Biol* 1 (2013) 394–397.
- [15] A. Cuadrado, G. Manda, A. Hassan, M.J. Alcaraz, C. Barbas, A. Daiber, P. Ghezzi, R. Leon, M.G. Lopez, B. Oliva, M. Pajares, A.I. Rojo, N. Robledinos-Anton, A.M. Valverde, E. Guney, H. Schmidt, Transcription factor NRF2 as a therapeutic target for chronic diseases: a systems medicine approach, *Pharmacol. Rev.* 70 (2018) 348–383.
- [16] M. Dodson, M.R. de la Vega, A.B. Cholanians, C.J. Schmidlin, E. Chapman, D.D. Zhang, Modulating NRF2 in disease: timing is everything, *Annu. Rev. Pharmacol. Toxicol.* 59 (2019) 555–575.
- [17] N. Keleku-Lukwete, M. Suzuki, M. Yamamoto, An overview of the advantages of KEAP1-NRF2 system Activation during inflammatory disease treatment, *Antioxidants Redox Signal.* 29 (2018) 1746–1755.
- [18] L. Virag, R.I. Jaen, Z. Regdon, L. Bosca, P. Prieto, Self-defense of macrophages against oxidative injury: fighting for their own survival, *Redox Biol* 26 (2019) 101261.
- [19] L. Baird, D. Lleres, S. Swift, A.T. Dinkova-Kostova, Regulatory flexibility in the Nrf2-mediated stress response is conferred by conformational cycling of the Keap1-Nrf2 protein complex, *Proc. Natl. Acad. Sci. U.S.A.* 110 (2013) 15259–15264.
- [20] L. Baird, S. Swift, D. Lleres, A.T. Dinkova-Kostova, Monitoring Keap1-Nrf2 interactions in single live cells, *Biotechnol. Adv.* 32 (2014) 1133–1144.
- [21] B.L. Hopkins, C.A. Neumann, Redoxins as gatekeepers of the transcriptional oxidative stress response, *Redox Biol* 21 (2019) 101104.
- [22] A.J. Wilson, J.K. Kerns, J.F. Callahan, C.J. Moody, Keap calm, and carry on covalently, *J. Med. Chem.* 56 (2013) 7463–7476.
- [23] B.C. Dickinson, C. Huynh, C.J. Chang, A palette of fluorescent probes with varying emission colors for imaging hydrogen peroxide signaling in living cells, *J. Am. Chem. Soc.* 132 (2010) 5906–5915.
- [24] M.-C. Lu, J.-A. Ji, Z.-Y. Jiang, Q.-D. You, The keap1–nrf2–ARE pathway as a potential preventive and therapeutic target: an update, *Med. Res. Rev.* 36 (2016) 924–963.
- [25] A. Cuadrado, A.I. Rojo, G. Wells, J.D. Hayes, S.P. Cousin, W.L. Rumsey, O.C. Attucks, S. Franklin, A.L. Levenon, T.W. Kensler, A.T. Dinkova-Kostova, Therapeutic targeting of the NRF2 and KEAP1 partnership in chronic diseases, *Nat. Rev. Drug Discov.* 18 (2019) 295–317.
- [26] Z. Jiang, M. Lu, Q.D. You, Discovery and development of kelch-like ECH-associated protein 1: nuclear factor erythroid 2-related factor 2 (KEAP1:NRF2) protein-protein interaction inhibitors: achievements, challenges and future directions, *J. Med. Chem.* 59 (2016) 10837–10858.
- [27] J.S. Pallesen, K.T. Tran, A. Bach, Non-covalent small-molecule kelch-like ECH-associated protein 1-nuclear factor erythroid 2-related factor 2 (Keap1-Nrf2) inhibitors and their potential for targeting central nervous system diseases, *J. Med. Chem.* 61 (2018) 8088–8103.

- [28] P. Liu, W. Tian, S. Tao, J. Tillotson, E.M.K. Wijeratne, A.A.L. Gunatilaka, D.D. Zhang, E. Chapman, Non-covalent NRF2 activation confers greater cellular protection than covalent activation, *Cell Chem. Biol.* 26 (2019) 1427–1435, e1425.
- [29] Y. Zhang, Z. Shi, Y. Zhou, Q. Xiao, H. Wang, Y. Peng, Emerging substrate proteins of kelch-like ECH associated protein 1 (Keap1) and potential challenges for the development of small-molecule inhibitors of the keap1-nuclear factor erythroid 2-related factor 2 (Nrf2) protein-protein interaction, *J. Med. Chem.* (2020), <https://doi.org/10.1021/acs.jmedchem.9b01865>.
- [30] H. Zhou, Y. Wang, Q. You, Z. Jiang, Recent progress in the development of small molecule Nrf2 activators: a patent review (2017–present), *Expert Opin. Ther. Pat.* 30 (2020) 209–225.
- [31] C.H. Leung, J.T. Zhang, G.J. Yang, H. Liu, Q.B. Han, D.L. Ma, Emerging screening approaches in the development of nrf2-keap1 protein-protein interaction inhibitors, *Int. J. Mol. Sci.* 20 (2019).
- [32] R. Hancock, H.C. Bertrand, T. Tsujita, S. Naz, A. El-Bakry, J. Laoruchpong, J.D. Hayes, G. Wells, Peptide inhibitors of the Keap1-Nrf2 protein-protein interaction, *Free Radic. Biol. Med.* 52 (2012) 444–451.
- [33] M.-C. Lu, Z.-W. Yuan, Y.-L. Jiang, Z.-Y. Chen, Q.-D. You, Z.-Y. Jiang, A systematic molecular dynamics approach to the study of peptide Keap1-Nrf2 protein-protein interaction inhibitors and its application to p62 peptides, *Mol. Biosyst.* 12 (2016) 1378–1387.
- [34] R. Hancock, M. Schaap, H. Pfister, G. Wells, Peptide inhibitors of the Keap1-Nrf2 protein-protein interaction with improved binding and cellular activity, *Org. Biomol. Chem.* 11 (2013) 3553–3557.
- [35] M. Lu, Z. Chen, Y. Wang, Y. Jiang, Z. Yuan, Q. You, Z. Jiang, Binding thermodynamics and kinetics guided optimization of potent keap1-nrf2 peptide inhibitors, *RSC Adv.* 5 (2015) 85983–85987.
- [36] S. Sogabe, K. Sakamoto, Y. Kamada, A. Kadotani, Y. Fukuda, J.I. Sakamoto, Discovery of a Kelch-like ECH-associated protein 1-inhibitory tetrapeptide and its structural characterization, *Biochem. Biophys. Res. Commun.* 486 (2017) 620–625.
- [37] N.D. Georgakopoulos, S.K. Talapatra, J. Gatiloff, F. Kozielski, G. Wells, Modified peptide inhibitors of the keap1-nrf2 protein-protein interaction incorporating unnatural amino acids, *ChemBiochem* 19 (2018) 1810–1816.
- [38] H. Salim, J. Song, A. Sahni, D. Pei, Development of a cell-permeable cyclic peptidyl inhibitor against the keap1-nrf2 interaction, *J. Org. Chem.* 85 (2019) 1416–1424.
- [39] L. Hu, S. Magesh, L. Chen, L. Wang, T.A. Lewis, Y. Chen, C. Khodier, D. Inoyama, L.J. Beamer, T.J. Emge, J. Shen, J.E. Kerrigan, A.N. Kong, S. Dandapani, M. Palmer, S.L. Schreiber, B. Munoz, Discovery of a small-molecule inhibitor and cellular probe of Keap1-Nrf2 protein-protein interaction, *Bioorg. Med. Chem. Lett* 23 (2013) 3039–3043.
- [40] E. Jnoff, C. Albrecht, J.J. Barker, O. Barker, E. Beaumont, S. Bromidge, F. Brookfield, M. Brooks, C. Bubert, T. Ceska, V. Corden, G. Dawson, S. Ducloux, T. Fryatt, C. Genicot, E. Jigorel, J. Kwong, R. Maghames, I. Mushi, R. Pike, Z.A. Sands, M.A. Smith, C.C. Stimson, J.P. Courade, Binding mode and structure-activity relationships around direct inhibitors of the Nrf2-Keap1 complex, *ChemMedChem* 9 (2014) 699–705.
- [41] C. Zhuang, S. Narayanapillai, W. Zhang, Y.Y. Sham, C. Xing, Rapid identification of Keap1-Nrf2 small-molecule inhibitors through structure-based virtual screening and hit-based substructure search, *J. Med. Chem.* 57 (2014) 1121–1126.
- [42] H.C. Bertrand, M. Schaap, L. Baird, N.D. Georgakopoulos, A. Fowkes, C. Thiollier, H. Kachi, A.T. Dinkova-Kostova, G. Wells, Design, synthesis, and evaluation of triazole derivatives that induce Nrf2 dependent gene products and inhibit the keap1-nrf2 protein-protein interaction, *J. Med. Chem.* 58 (2015) 7186–7194.
- [43] N. Meng, H. Tang, H. Zhang, C. Jiang, L. Su, X. Min, W. Zhang, H. Zhang, Z. Miao, W. Zhang, C. Zhuang, Fragment-growing guided design of Keap1-Nrf2 protein-protein interaction inhibitors for targeting myocarditis, *Free Radic. Biol. Med.* 117 (2018) 228–237.
- [44] D.A. Abed, S. Lee, L. Hu, Discovery of disubstituted xylene derivatives as small molecule direct inhibitors of Keap1-Nrf2 protein-protein interaction, *Bioorg. Med. Chem.* 28 (2020) 115343.
- [45] S. Kim, A.N. Indu Viswanath, J.H. Park, H.E. Lee, A.Y. Park, J.W. Choi, H.J. Kim, A.M. Londhe, B.K. Jang, J. Lee, H. Hwang, S.M. Lim, A.N. Pae, K.D. Park, Nrf2 activator via interference of Nrf2-Keap1 interaction has antioxidant and anti-inflammatory properties in Parkinson's disease animal model, *Neuropharmacology* 167 (2020) 107989.
- [46] P.R. Lazzara, A.D. Jain, A.C. Maldonado, B. Richardson, K.J. Skowron, B.P. David, Z. Siddiqui, K.M. Ratia, T.W. Moore, Synthesis and evaluation of noncovalent naphthalene-based KEAP1-NRF2 inhibitors, *ACS Med. Chem. Lett.* 11 (2020) 521–527.
- [47] Z.-Y. Jiang, M.-C. Lu, L.L. Xu, T.-T. Yang, M.-Y. Xi, X.-L. Xu, X.-K. Guo, X.-J. Zhang, Q.-D. You, H.-P. Sun, Discovery of potent keap1-nrf2 protein-protein interaction inhibitor based on molecular binding determinants analysis, *J. Med. Chem.* 57 (2014) 2736–2745.
- [48] T.G. Davies, W.E. Wixted, J.E. Coyle, C. Griffiths-Jones, K. Hearn, R. McMenamin, D. Norton, S.J. Rich, C. Richardson, G. Saxty, H.M.G. Willems, A.J.A. Woolford, J.E. Cottom, J.-P. Kou, J.G. Yonchuk, H.G. Feldser, Y. Sanchez, J.P. Foley, B.J. Bolognese, G. Logan, P.L. Podolin, H. Yan, J.F. Callahan, T.D. Heightman, J.K. Kerns, Monoacidic inhibitors of the kelch-like ECH-associated protein 1: nuclear factor erythroid 2-related factor 2 (KEAP1:NRF2) protein-protein interaction with high cell potency identified by fragment-based discovery, *J. Med. Chem.* 59 (2016) 3991–4006.
- [49] T.D. Heightman, J.F. Callahan, E. Chiarparin, J.E. Coyle, C. Griffiths-Jones, A.S. Lakdawala, R. McMenamin, P.N. Mortenson, D. Norton, T.M. Peakman, S.J. Rich, C. Richardson, W.L. Rumsey, Y. Sanchez, G. Saxty, H.M.G. Willems, L. Wolfe 3rd, A.J. Woolford, Z. Wu, H. Yan, J.K. Kerns, T.G. Davies, Structure-activity and structure-conformation relationships of aryl propionic acid inhibitors of the kelch-like ECH-associated protein 1/nuclear factor erythroid 2-related factor 2 (KEAP1/NRF2) protein-protein interaction, *J. Med. Chem.* 62 (2019) 4683–4702.
- [50] P.R. Lazzara, B.P. David, A. Ankireddy, B. Richardson, K. Dye, K.M. Ratia, S.P. Reddy, T.W. Moore, Isoquinoline kelch-like ECH-associated protein 1-nuclear factor (Erythroid-derived 2)-like 2 (KEAP1-NRF2) inhibitors with high metabolic stability, *J. Med. Chem.* (2019), <https://doi.org/10.1021/acs.jmedchem.9b01074>.
- [51] B. Ma, B. Lucas, A. Capacci, E.Y. Lin, J.H. Jones, M. Dechantsreiter, I. Enyedy, D. Marcotte, G. Xiao, B. Li, K. Richter, Design, synthesis and identification of novel, orally bioavailable non-covalent Nrf2 activators, *Bioorg. Med. Chem. Lett* 30 (2020) 126852.
- [52] C. Gorgulla, A. Boeszoeremnyi, Z.F. Wang, P.D. Fischer, P. Coote, K.M. Padmanabha Das, Y.S. Malets, D.S. Radchenko, Y.S. Moroz, D.A. Scott, K. Fackeldey, M. Hoffmann, I. Javniuk, G. Wagner, H. Arthanari, An open-source drug discovery platform enables ultra-large virtual screens, *Nature* (2020), <https://doi.org/10.1038/s41586-020-2117-z>.
- [53] M.-C. Lu, J.-A. Ji, Y.-L. Jiang, Z.-Y. Chen, Z.-W. Yuan, Q.-D. You, Z.-Y. Jiang, An inhibitor of the Keap1-Nrf2 protein-protein interaction protects NCM460 colonic cells and alleviates experimental colitis, *Sci. Rep.* 6 (2016) 26585.
- [54] Q. Hui, M. Karlstetter, Z. Xu, J. Yang, L. Zhou, H.M. Eilken, C. Terjung, H. Cho, J. Gong, M.J. Lai, K. Nassar, E.J. Duh, Inhibition of the Keap1-Nrf2 protein-protein interaction protects retinal cells and ameliorates retinal ischemia-reperfusion injury, *Free Radical Biol. Med.* 146 (2020) 181–188.
- [55] F. Kerr, O. Sofola-Adesakin, D.K. Ivanov, J. Gatiloff, B. Gomez Perez-Nieves, H.C. Bertrand, P. Martinez, R. Callard, I. Snoeren, H.M. Cocheme, J. Adcott, M. Khericha, J.J. Castillo-Quan, G. Wells, W. Noble, J. Thornton, L. Partridge, Direct Keap1-Nrf2 disruption as a potential therapeutic target for Alzheimer's disease, *PLoS Genet.* 13 (2017) e1006593.
- [56] M.C. Lu, J. Zhao, Y.T. Liu, T. Liu, M.M. Tao, Q.D. You, Z.Y. Jiang, CPUY192018, a potent inhibitor of the Keap1-Nrf2 protein-protein interaction, alleviates renal inflammation in mice by restricting oxidative stress and NF-kappaB activation, *Redox Biol* 26 (2019) 101266.
- [57] D. Marcotte, W. Zeng, J.-C. Hus, A. McKenzie, C. Hession, P. Jin, C. Bergeron, A. Lugovskoy, I. Enyedy, H. Cuervo, D. Wang, C. Atmanene, D. Roeklin, M. Vecchi, V. Vivat, J. Kraemer, D. Winkler, V. Hong, J. Chao, M. Lukashev, L. Silvan, Small molecules inhibit the interaction of Nrf2 and the Keap1 Kelch domain through a non-covalent mechanism, *Bioorg. Med. Chem.* 21 (2013) 4011–4019.
- [58] Z.Y. Jiang, L.L. Xu, M.C. Lu, Z.Y. Chen, Z.W. Yuan, X.L. Xu, X.K. Guo, X.J. Zhang, H.P. Sun, Q.D. You, Structure-activity and structure-property relationship and exploratory in vivo evaluation of the nanomolar keap1-nrf2 protein-protein interaction inhibitor, *J. Med. Chem.* 58 (2015) 6410–6421.
- [59] M.-C. Lu, S.-J. Tan, J.-A. Ji, Z.-Y. Chen, Z.-W. Yuan, Q.-D. You, Z.-Y. Jiang, Polar recognition group study of keap1-nrf2 protein-protein interaction inhibitors, *ACS Med. Chem. Lett.* 7 (2016) 835–840.
- [60] A.D. Jain, H. Potteti, B.G. Richardson, L. Kingsley, J.P. Luciano, A.F. Ryuzoji, H. Lee, A. Krunic, A.D. Mesecar, S.P. Reddy, T.W. Moore, Probing the structural requirements of non-electrophilic naphthalene-based Nrf2 activators, *Eur. J. Med. Chem.* 103 (2015) 252–268.
- [61] A.F. Winkel, C.K. Engel, D. Margerie, A. Kannt, H. Szillat, H. Glombik, C. Kallus, S. Ruf, S. Gussregen, J. Riedel, A.W. Herling, A. von Knethen, A. Weigert, B. Brune, D. Schmoll, Characterization of RA839, a noncovalent small molecule binder to Keap1 and selective activator of Nrf2 signaling, *J. Biol. Chem.* 290 (2015) 28446–28455.
- [62] M.C. Lu, X. Zhang, F. Wu, S.J. Tan, J. Zhao, Q.D. You, Z.Y. Jiang, Discovery of a potent kelch-like ECH-associated protein 1-nuclear factor erythroid 2-related factor 2 (Keap1-Nrf2) protein-protein interaction inhibitor with natural proline structure as a cytoprotective agent against acetaminophen-induced hepatotoxicity, *J. Med. Chem.* 62 (2019) 6796–6813.
- [63] B.G. Richardson, A.D. Jain, T.E. Speltz, T.W. Moore, Non-electrophilic modulators of the canonical Keap1/Nrf2 pathway, *Bioorg. Med. Chem. Lett* 25 (2015) 2261–2268.